Human Molecular Genetics, 2001, Vol. 10, No. 17 **1829–1845**

Polyglutamine expansions cause decreased CRE-mediated transcription and early gene expression changes prior to cell death in an inducible cell model of Huntington's disease

Andreas Wyttenbach, Jina Swartz, Hiroko Kita[1], Thomas Thykjaer[2], Jenny Carmichael, Jane Bradley[3], Rosemary Brown, Michelle Maxwell, Anthony Schapira[3], Torben F. Orntoft[2], Kikuya Kato[1] and David C. Rubinsztein*

Wellcome Trust Centre for Molecular Mechanisms in Disease, Cambridge Institute for Medical Research, Wellcome Trust/MRC Building, Addenbrooke's Hospital, Hills Road, Cambridge CB2 2XY, UK, [1]Taisho Laboratory of Functional Genomics, Nara Institute of Science and Technology, 8916-5 Takayama, Ikoma, Nara, 630-0101, Japan, [2]Molecular Diagnostic Laboratory, Department of Clinical Biochemistry, Aarhus University Hospital, Brendstrupgaardsvej, 8200 Aarhus N., Denmark and [3]University Department of Clinical Neurosciences, Royal Free and University College Medical School, UCL, London NW3 2PF, and Institute of Neurology, Queen Square, London WC1N 3BG, UK

Received May 8, 2001; Revised and Accepted June 19, 2001

Huntington's disease (HD) is one of 10 known diseases caused by a $(CAG)_n$ trinucleotide repeat expansion that is translated into an abnormally long polyglutamine tract. We have developed stable inducible neuronal (PC12) cell lines that express huntingtin exon 1 with varying CAG repeat lengths under doxycycline (dox) control. The expression of expanded repeats is associated with aggregate formation, caspase-dependent cell death and decreased neurite outgrowth. Post-mitotic cells expressing mutant alleles were more prone to cell death compared with identical cycling cells. To determine early metabolic changes induced by this mutation in cell models, we studied changes in gene expression after 18 h dox induction, using Affymetrix arrays, cDNA filters and adapter-tagged competitive PCR (ATAC-PCR). At this time point there were low rates of inclusion formation, no evidence of mitochondrial compromise and no excess cell death in the lines expressing expanded compared with wild-type repeats. The expression profiles suggest novel targets for the HD mutation and were compatible with impaired cAMP response element (CRE)-mediated transcription, which we confirmed using CRE-luciferase reporter assays. Reduced CRE-mediated transcription may contribute to the loss of neurite outgrowth and cell death in polyglutamine diseases, as these phenotypes were partially rescued by treating cells with cAMP or forskolin.

INTRODUCTION

Huntington's disease (HD) is a progressive, autosomal dominant, neurodegenerative disorder caused by a CAG trinucleotide repeat expansion in the gene that encodes huntingtin (htt) (1). Symptomatic individuals have 36 or more repeats and the length of the trinucleotide expansion tends to be inversely correlated with the age of onset. The CAG expansion is translated into a series of glutamine residues [a polyglutamine (polyQ) tract] in htt. HD is one of 10 known neurodegenerative disorders, including spinobulbar muscular atrophy (SBMA), dentatorubral pallidolusian atrophy (DRPLA) and five forms of spinocerebellar ataxia (SCA), caused by a polyQ expansion (reviewed in 2–4).

PolyQ diseases are characterized by neuronal loss and intraneuronal aggregates/inclusions containing the respective gene products or fragments including the polyQ tract (reviewed in 2). The pathogenic roles of aggregates/aggregation are subjects of vigorous debate (5–9). The earliest clinical signs of these diseases may be due to cell dysfunction that occurs before overt cell loss. In studies of SCA1 transgenic mice, the earliest clinical deficits correlate with the loss of dendritic spines, which precede cell loss (10). Loss of dendritic spines is also a feature of HD pathology (11).

In order to model the biology of polyglutamine diseases in tissue culture, we have generated inducible lines in PC12 (rat phaeochromocytoma) cells, which express a GFP-tagged exon 1 fragment of the HD gene with 23, 43, 53 or 74 glutamine repeats, driven by a doxycycline (dox)-dependent Tet-On promoter (12). PolyQ diseases have been extensively studied using htt exon 1, because large fragments of the HD, SCA3 and DRPLA gene products do not induce inclusion formation or cell death in cell culture models (13–17). Also, a

*To whom correspondence should be addressed. Tel: +44 1223 762608; Fax: +44 1223 331206; Email: dcr1000@cus.cam.ac.uk
The authors wish it to be known that, in their opinion, the first two authors should be regarded as joint First Authors.

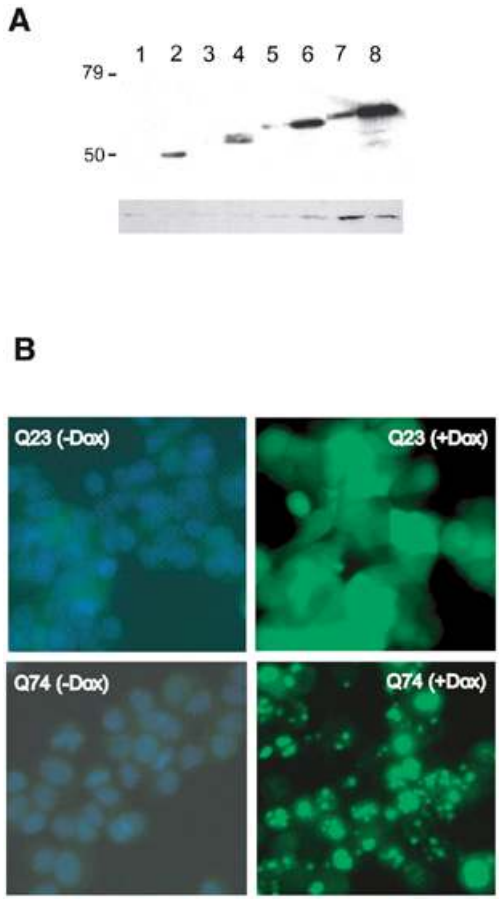

Figure 1. Western blot and immunofluorescence of inducible PC12 cell lines. (**A**) Western blot of total cell extracts obtained from HD-Q23, -Q43, -Q53 and -Q74 cell lines. Similar amounts of protein extracts were run on a 12% polyacrylamide gel, blotted and incubated with anti-EGFP antibody (1:1000). Cells were either not treated (Q23, lane 1; Q43, lane 3; Q53, lane 5; Q74, lane 7) or treated with 1 µg/ml of dox for 24 h (Q23, lane 2; Q43, lane 4; Q53, lane 6; Q74, lane 8). Loading is controlled by blotting against actin (lower bands). (**B**) Immunofluorescence of PC12 cells stably transfected with htt exon 1 fused to the EGFP with either 23 or 74 glutamines (HD-Q23 and -Q74). Cells were grown on coverslips in the absence (–Dox) or presence of 1000 ng/ml of dox (+Dox) for 48 h, fixed and nuclei stained with DAPI (blue). Insoluble aggregates produced by HD-Q74 cells appear as bright EGFP signals that are distinct from non-aggregated EGFP in HD-Q23 cells (see Results for details).

small N-terminal polyQ-containing part(s) of htt is found in inclusions *in vivo* (18). Exon 1 models have been powerful tools for studying inclusion formation in relation to cell death/dysfunction in cultured cells and transgenic mice (19–22). While these models may not reflect the cellular specificity of HD, they are likely to show features generic to all polyglutamine diseases. These diseases almost certainly share common pathogenic pathways, and an understanding of the shared pathways will have a wide impact on the biology of neurodegenerative processes.

In this study we report the basic characterization of the inducible lines, where we have specifically investigated susceptibility to cell death and htt aggregation. It is possible that the post-mitotic state of virtually all neurons contributes to the central nervous system (CNS) being more susceptible to polyQ mutations than many other tissues expressing the mutant proteins. Accordingly, we compared cell death and inclusion formation in the same clonal cell lines in cycling and post-mitotic states. Proteasome inhibition increases polyQ aggregate formation and inclusions sequester ubiquitin, proteasomal components and heat-shock proteins (HSPs) *in vivo* (20,23–25). We studied the kinetics of the association of these components with the aggregates, since some proteins may be sequestered to inclusions as late events long after their formation.

One of our aims is to determine the earliest metabolic changes resulting from the HD mutation. We have studied mRNA expression profiles in our PC12 cell lines at an early time after induction of expression, in order to preferentially assay the primary consequences of polyQ mutations, as opposed to secondary downstream effects. PC12 cells were chosen as these neuronal precursor cells have been extensively characterized. The use of clonal cell lines allows comparisons of cells of common origin under conditions of fairly homogenous transgene expression, where the main difference between the lines is the length of the polyQ tract. (Since integration sites also differ between lines, we have repeated relevant experiments in independent clonal lines.) We believe that this approach is a powerful strategy, which complements gene expression studies in transgenic mice (26). As far as we are aware, this is the first report of mRNA profiling in a cellular model of a polyQ disease or a neurodegenerative condition associated with protein aggregation.

RESULTS

Inducible htt exon 1 expression leads to time- and polyQ length-dependent aggregation of insoluble, fibrillar inclusions

We established stable, inducible PC12 cell lines, where expression of htt exon 1 containing 23, 43, 53 or 74 glutamines (HD-Q23, -Q43, -Q53 or -Q74) fused downstream of enhanced green fluorescent protein (EGFP) is driven by a minimal cytomegalovirus promoter under the control of a tetracycline responsive element (TRE). This promoter is induced when the 'reverse' Tet repressor (tTetR) binds to TRE in the presence of dox. We grew 20–40 independent single cell clones for each polyQ line and selected one inducible line from 2–4 low background/high inducer lines of each polyQ length for detailed study. Upon treatment with nerve growth factor (NGF) (100 ng/ml) in the presence of reduced amounts of serum (1%), each clonal cell line differentiated into post-mitotic, neuron-like cells in the absence of dox (data not shown).

In the absence of dox, the selected clonal lines expressed the htt exon 1 fragment at low levels as shown by western blotting (Fig. 1A). Induction with dox resulted in much higher levels of expression (Fig. 1A and B) and the htt exon 1 fragments expressed in HD-Q23, -Q43, -Q53 or -Q74 cell lines migrated as bands of increasing molecular weight on a polyacrylamide gel (>50 kDa, Fig. 1A). After induction, EGFP fluorescence localized to both the cytoplasm and nucleus in all clonal lines at early (8 h) and late (48 h) time points (Fig. 1B and data not shown). We examined 10–15 clonal lines (grown from single cells) for each polyQ stretch and found that low background expression ('leakiness' of the inducible promoter) occurred in all cases (data not shown). Please note that the apparently higher background signal in the HD-Q74 uninduced line

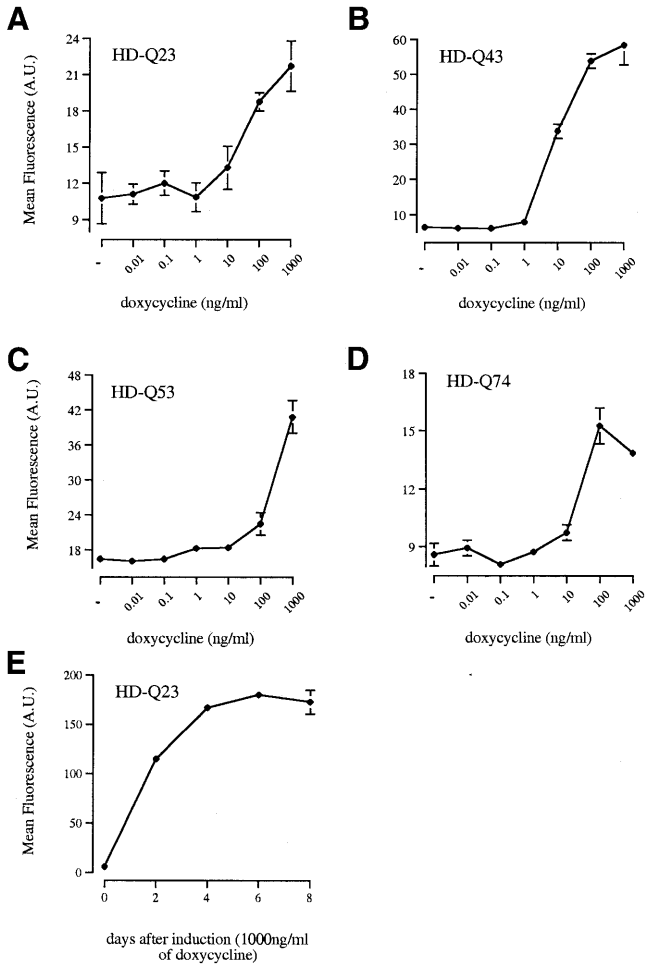

Figure 2. Dox dose dependence of transgene induction of inducible PC12 cell lines. (**A**) HD-Q23; (**B**) HD-Q43; (**C**) HD-Q53; (**D**) HD-Q74; expression was measured by the amount of EGFP expressed in a constant number of cells analysed by flow cytometry after exposure to different doses of dox for 8 h (A–D). Mean values of a.u. are represented from one triplicate experiment. (**E**) Expression levels of htt exon 1 containing 23 glutamines (HD-Q23 cell line) over an 8 day period.

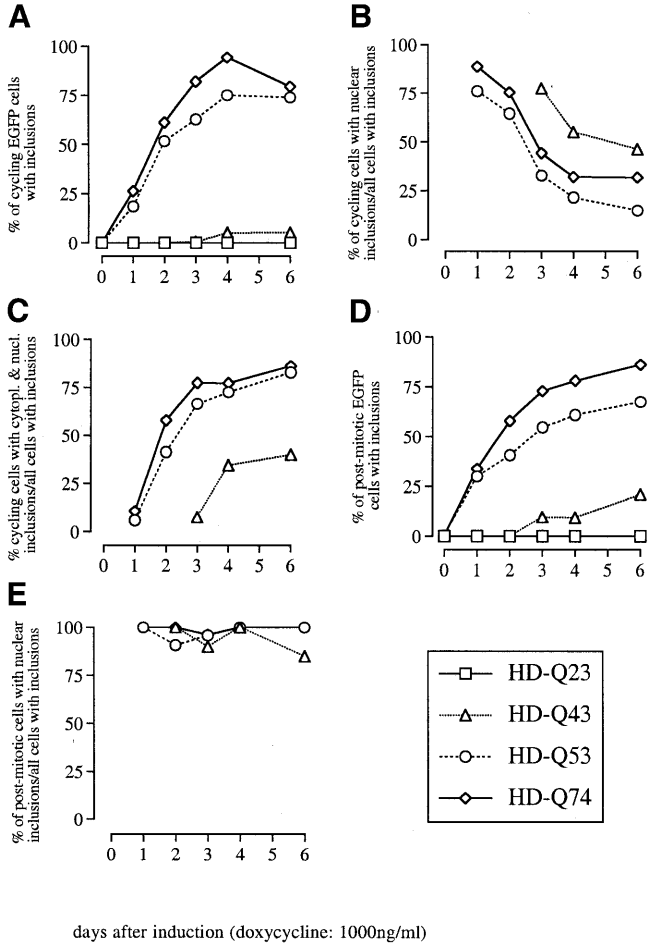

Figure 3. PolyQ length-dependent aggregation and intracellular localization of polyQ aggregates in cycling and post-mitotic inducible PC12 cells. (**A**) Proportion of EGFP-positive HD-Q23, -Q43, -Q53 and -Q74 cycling cells that contained inclusions. No aggregates were found in HD-Q23 cells. (**B**) Proportion of inclusion-containing HD-Q43, -Q53 and -Q74 cycling cells with only nuclear localization of inclusions. (**C**) Proportion of inclusion-containing HD-Q43, -Q53 and -Q74 cycling cells with both cytoplasmic and nuclear localization of inclusions. (**D**) Proportion of EGFP-positive HD-Q23, -Q43, -Q53 and -Q74 post-mitotic cells containing inclusions. (**E**) Proportion of inclusions containing HD-Q43, -Q53 and -Q74 post-mitotic cells with only nuclear localization of inclusions.

(Fig. 1A, lane 7) is largely due to the increased protein loading (assessed by actin probing on the figure).

Transgene expression in selected HD-Q23, -Q43, -Q53 and -Q74 lines measured 8 h after induction by EGFP fluorescence was dox dose dependent (Fig. 2A–D). EGFP fluorescence increased ~2–5-fold from an uninduced to an induced state after 8 h of dox treatment (1 μg/ml). To assess expression levels over longer time periods, we treated HD-Q23 cells with dox for up to 8 days. We chose HD-Q23 for this experiment since these cells never produce aggregates (see below); aggregated EGFP within cells results in a lower fluorescence intensity analysed by flow cytometry compared to an equal amount of uniformly distributed EGFP. Figure 2E shows that in HD-Q23 cells, transgene expression rose from six arbitrary units (a.u.) (uninduced state) to 180 a.u. at day 6 (30-fold difference). In most lines, the highest expression was observed with 1 μg/ml dox. In the HD-Q74 line, the expression was similar with 100 ng/ml and 1 μg/ml dox. Thus, in all subsequent experiments cells were induced with dox at 1 μg/ml.

Aggregates appeared as bright EGFP signals that were distinct from the diffuse, non-aggregated transgene when analysed by fluorescence microscopy (Fig. 1B). These visible aggregates can be clearly distinguished from homogenous EGFP expression seen in HD-Q23 cells and their presence or absence is unambiguous, as shown previously (20,27). Inclusion formation in clonal lines expressing expanded polyQ was time and polyQ length dependent in cycling cells (Fig. 3A) and NGF-differentiated, post-mitotic cells (Fig. 3D). A 14 day induction period was needed to obtain 90% of Q43 cells containing inclusions (cycling state, data not shown). No inclusions (HD-Q23 or -Q43), or very low levels of cells with inclusions (HD-Q53 or -Q74, <1%) were observed in the uninduced state.

In cycling cells that contained inclusions, the proportion of cells with exclusively nuclear localization of inclusions

decreased progressively over time after induction with dox (Fig. 3B). The proportion of cells in which inclusions were observed in the cytoplasm increased with time (Fig. 3C). The majority of cells (>85%) with cytoplasmic aggregates also contained inclusions in the nucleus. However, in NGF-differentiated, post-mitotic cells, inclusions localized mainly to the nucleus and we observed no change over time (Fig. 3E) in contrast to cycling cells (Fig. 3B). Occasionally, aggregates in post-mitotic cells localized to the cell soma or were found in neurites (data not shown).

To test whether the EGFP inclusions observed under the microscope were insoluble aggregates (which were not present in HD-Q23 cells), we treated HD-Q23 and HD-Q74 cells with Triton X-100 and SDS *in situ* after 48 h of induction with dox. As shown by Kazantsev *et al*. (28) inclusions can retain their fluorescence when insoluble. No fluorescent aggregates were detected for HD-Q23 cells after simultaneous treatment with Triton X-100 and SDS (0.1 or 4%) for 2 min. However, EGFP-fluorescent aggregates were seen for HD-Q74 cells treated for up to 3 weeks with 4% Triton X-100 and SDS (data not shown) showing that these polyQ aggregates were highly insoluble. Electron microscopy (EM) analysis of HD-Q74 cells treated with dox for 48 h showed aggregates that were of fibrillar structure (Fig. 4). Such aggregates were not found in cells expressing HD-Q23.

Time-dependent sequestration of components of the ubiquitin-proteasome pathway (UPP) and HSP 40 and 70 chaperones into inclusions in cycling and post-mitotic cells

On day 1–2 after induction of HD-Q74 cells, ubiquitin localized to inclusions in <1% of cells with inclusions, but at day 3–4 and day 6–7 we detected progressively more cells with ubiquitin-positive inclusions (Table 1). Ubiquitination was not correlated with the size of inclusions, but inclusions were more frequently ubiquitinated in cells that showed a reduction or absence of diffuse EGFP staining. Some cells with large inclusions appeared to have sequestered all of their EGFP into aggregates leaving no obvious fluorescence signal in the cytoplasm or nucleus outside the inclusions. These results indicate that ubiquitination is a 'late' event or that epitopes are hidden earlier on. The only other component of the UPP tested in this study that strongly localized to inclusions was the 20S proteasome. The 20S proteasome component co-localized with inclusions in >50% of cells with inclusions at day 1–2 following induction and this level of co-localization remained constant over time (Table 1). In HD-Q74 cells, 20S proteasome colocalized similarly to small and large inclusions (data not shown). Antibodies directed to the 11S α-subunit occasionally localized to inclusions at day 6–7 (Table 1). Antibodies directed against epitopes of the E2 conjugating enzyme, the 19S (p45) proteasome and the β- and γ-subunit of the 11S proteasome did not localize with inclusions.

Members of the HSP40/70 family of chaperones (HDJ-1, HDJ-2, HSC70 and HSP70) localized to inclusions (Table 1 and data not shown). The proportion of cells with HSP-positive inclusions did not markedly change over a 6–7 day period for cycling and post-mitotic HD-Q74 cells (Table 1). These HSPs localized to inclusions irrespective of their intracellular location (nuclear or cytoplasmic) (data not shown). We did not find any obvious difference in the levels of endogenous HSP staining between cells with or without inclusions. However, we noted that dying cells (rounded and shrunken cell body) gave a strong cytoplasmic and nuclear signal for HSP70, compatible with induction of this HSP, as suggested by Chai *et al*. (24 and data not shown). We did not detect any redistribution of HSP27, HSP90 and HSP110 into inclusions in cycling or post-mitotic HD-Q74 PC12 cells (Table 1).

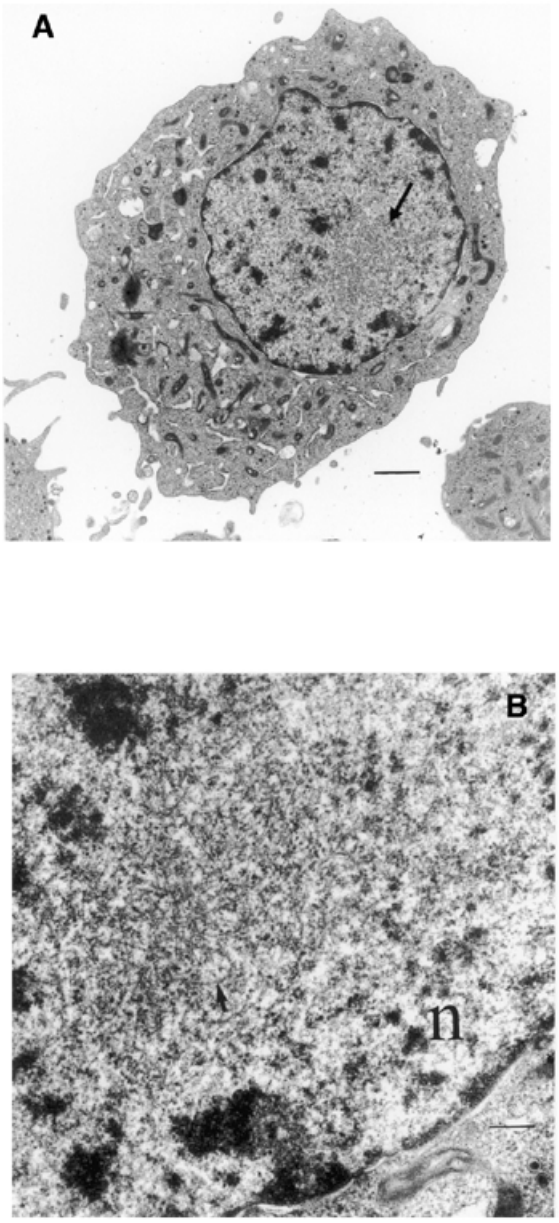

Figure 4. Fibrillar structure of polyQ aggregates in inducible PC12 cells. (**A**) Electron micrograph showing an HD-Q74 PC12 cell after 48 h of dox treatment containing an aggregate (arrow) in the nucleus. Such aggregated structures were not found in HD-Q23 cells. Scale bar, 1 μm. (**B**) High magification of aggregate in (A) showing the fibrillar structure of the inclusion. Arrow points to a fibrillar structure. n, nucleus. Scale bar, 250 nm.

Expression of htt exon 1 with a polyQ expansion causes moderate caspase-dependent cell death in cycling cells

In cycling cells, >90% of cells were EGFP-positive after 24 h of induction and these cells could clearly be distinguished from

Table 1. Sequestration of components of the UPP and HSPs into polyQ aggregates of PC12 inducible HD-Q74 cells analysed by immunocytochemistry after various periods of dox treatment (1 μg/ml)

Antibody	Day 1–2	Day 3–4	Day 6–7
Ubiquitin	+/–	+	++
E2 conjugat.	–	–	–
11S α	–	–	+/–
11S β	–	–	–
11S γ	–	–	–
19S (p45)	–	–	–
20S	+++	+++	+++
HSP25	–	–	–
HSP27	–	–	–
HDJ-1	+++	+++	+++
HDJ-2	+++	+++	+++
HSC70	++	++	++
HSP70	+++	+++	+++
HSP90	–	–	–
HSP110	–	–	–

Data are representative of both cycling and post-mitotic cells.
+/–, Occasional co-localization (<1% of cells with inclusions); +, 1–10% of cells with inclusions; ++, 10–50% of cells with inclusions; +++, 50–100% of cells with inclusions; E2 conjugat., E2 ubiquitin conjugating enzyme; 11S, 19S, 20S, proteasome subunits; HSP, heat-shock protein; HSC, heat-shock cognate (non-inducible).

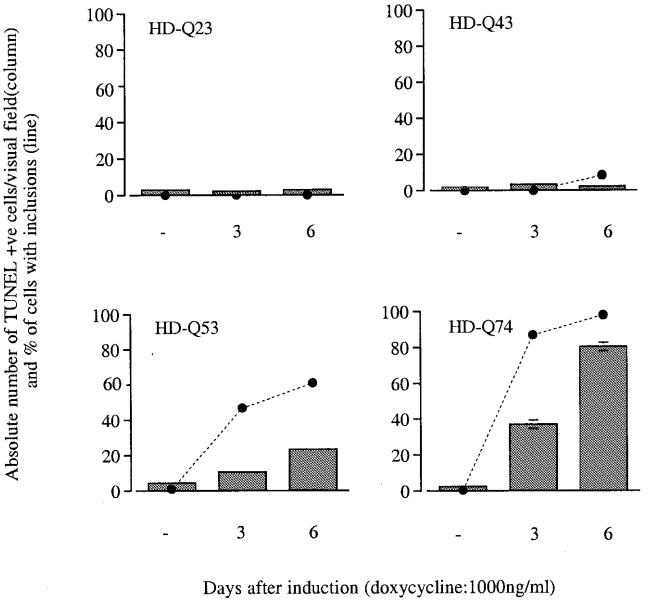

Figure 5. Time-course experiment using cycling HD-Q23, -Q43, -Q53 and -Q74 PC12 cells that were grown on coverslips for 6 days in the absence (–) or presence of 1000 ng/ml dox for 3 or 6 days. The viability of cells was examined by using TUNEL to visualize cells with DNA-strand breakage. Columns represent the absolute number of TUNEL-positive cells per visual field detected in 5–10 randomly chosen high power fields (40×). In all cases, we scored high power fields that were ~80% confluent. The dotted line represents the proportion of cells containing inclusions as a percentage (%), in the same experiment run in parallel. This experiment was performed three times with similar results and data from one representative experiment are shown.

uninduced cells. The ratio between induced (EGFP-positive) versus uninduced (EGFP-negative) cells in each stable line did not change over time (14 days) suggesting that there is no loss of inducibility over time and that virtually all cells expressed the transgene. Transgene induction over a 6 day period did not lead to detectable increases in cell death in HD-Q23 and -Q43 cells using the TdT-mediated-terminal-dUTP-nick-end-labelling (TUNEL) assay (Fig. 5A and B). However, overexpression of htt exon 1 in cells containing an HD-Q53 and -Q74 expansion resulted in more TUNEL-positive cells and this effect was strongest in HD-Q74 cells (Fig. 5C and D). We observed a positive correlation between the proportion of cells with inclusions and the presence of more TUNEL-positive cells (Fig. 5). We estimated that 15–20% of the HD-Q74 cell population induced for 6 days (1 μg/ml of dox) was TUNEL-positive compared with uninduced HD-Q74 cells (0.1%) or HD-Q74 cells treated with a low dose of dox (1 ng/ml, 0.7%) (Fig. 6A). This moderate amount of cell death in HD-Q74 occurred after the peak of aggregate formation was reached (Fig. 5 and data not shown).

The number of TUNEL-positive cycling cells expressing the polyQ mutation was significantly reduced by treatment with the broad caspase inhibitor zVAD-fmk, despite similar levels of inclusion formation (6 day induction) (Fig. 6A and B). We did not observe such a reduction in cell death using zDEVD-fmk (caspase 3-like inhibitor) or the solvent control (DMSO).

To confirm the moderate amount of cell death detected in HD-Q74 cells after transgene induction using the TUNEL assay (see above) we analysed the numbers of surviving HD-Q23 and HD-Q74 cycling cells initially seeded at identical densities at different times after induction using flow cytometry. Assuming a similar rate of cell division, there were ~84% of surviving HD-Q74 cells at day 4, ~75% HD-Q74 cells at day 6 and ~60% HD-Q74 cells at day 8, compared with surviving HD-Q23 cells (Fig. 7A).

Expression of htt exon 1 with a polyQ expansion increases cell death in post-mitotic cells and inhibits neurite outgrowth

We used inducible PC12 cells to investigate whether the rate of cell death observed in cycling cells was of similar magnitude in post-mitotic cells. For this purpose, we differentiated the same clonal PC12 cells used in the death assays described above (HD-Q23, -Q43, -Q53, -Q74) into post-mitotic, neuron-like cells using low serum culture medium and NGF. We first determined the number of living cells at day 6 after dox treatment and simultaneous NGF exposure using the trypan blue exclusion assay. In Figure 7B, the presence of living cells for each clonal line is expressed as the ratio between cells present after dox treatment versus no treatment. We observed extensive cell loss for HD-Q53 (~75%) and HD-Q74 (>80%) after dox treatment, while HD-Q23 and HD-Q43 did not show significant cell loss. These results were confirmed in two independent experiments and two cell lines of independent clonal origin expressing Q23 and Q74 expansions (data not shown). Cell loss correlated with repeat length ($R^2 = 0.74$; $P < 0.0001$; linear regression). No significant cell loss was detected for the

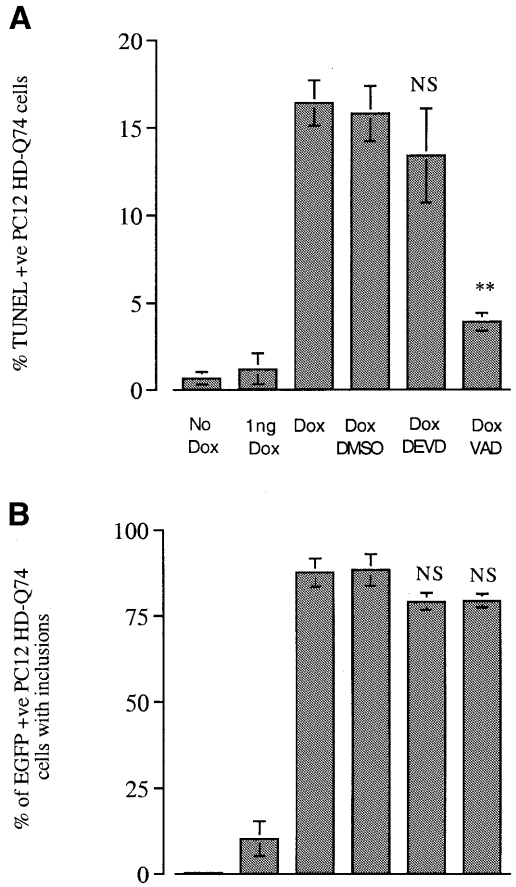

Figure 6. Cell death is reduced by the caspase inhibitor zVAD-fmk in PC12 cells. (**A**) Columns represent the proportion of TUNEL-positive cycling HD-Q74 cells (PC12) out of a whole cell population that was grown on coverslips for 6 days and not treated with dox (no Dox), treated with 1 ng/ml of dox or with 1000 ng/ml of dox (Dox) with addition of the general caspase inhibitor zVAD-fmk (100 μM), the caspase 3-like inhibitor zDEVD-fmk (200 μM) or the solvent control (DMSO). Means of three independent experiments with standard errors are shown. (**B**) Columns represent the proportion of EGFP-positive cells containing inclusions for three parallel experiments to (A), under the same conditions. Unpaired two-tailed *t*-tests were performed to test the effects of zVAD-fmk or zDEVD-fmk versus DMSO controls. $^{**}P < 0.001$; NS, $P > 0.05$.

HD-Q23 or parental Tet-On cells and there was no significant difference between the HD-Q23 and Tet-On lines ($P > 0.05$, unpaired *t*-test) (Fig. 7B).

We next examined whether polyQ expansions affected neurite outgrowth. In order to exclude the possibility that reduced neurite outgrowth was simply caused by cell death we focused on HD-Q23, -Q43, -Q53 and -Q74 cells with intact nuclei and normal cell volume/shape, grown in the presence or absence of dox and noted the degree of neurite extension. We found that cells stably expressing htt exon 1 with a polyQ expansion were less likely to show neurite outgrowth (Fig. 7C). This effect was also dependent on the length of the polyQ expansion. We obtained consistent results for HD-Q23 and -Q74 cells of different clonal origin (data not shown).

In post-mitotic cells, we observed an inverse correlation between neurite outgrowth and cell death measured as nuclear condensation or fragmentation. After 7 days of dox treatment, only 6% of HD-Q74 cells that developed neurites showed nuclear condensation/fragmentation, whereas 77% of HD-Q74 cells that did not develop neurites showed nuclear abnormalities. In post-mitotic cells with reduced neurite outgrowth, the proportion of dox-treated HD-Q53 and HD-Q74 cells with a condensed or fragmented nucleus was significantly different from non-treated cells and cell death was correlated with larger polyQ expansion ($R^2 = 0.84$; $P = 0.0002$; linear regression) (Fig. 7D). We did not detect any nuclear abnormalities in dox-treated post-mitotic HD-Q23 cells (Fig. 7D). Furthermore, we did not observe nuclear fragmentation in cycling HD-Q23 or HD-Q74 PC12 cells treated with dox (data not shown). Cell death in post-mitotic cells expressing expanded repeats was caspase dependent (Fig. 8A), as we observed with cycling cells. However, the broad caspase inhibitor zVAD-fmk did not improve the proportions of normal EGFP-positive HD-Q74 cells with neurite outgrowth (Fig. 8B), confirming that the decreased neurite outgrowth was not simply a consequence of cell death.

PolyQ expansions do not cause mitochondrial compromise at early times after induction of expression

A major aim of our study was to investigate early changes in gene expression in our inducible cell model. Since alterations in mitochondrial metabolism may occur in HD and in animal models (29,30), such changes may cause secondary changes in gene expression unrelated to the polyQ expansion. Thus, we took the precaution of ensuring that no overt defects were occuring at the times when we performed the gene expression studies. We determined a range of mitochondrial functions in the three independent HD-Q74 and three independent HD-Q23 cell lines that were used in the various gene expression assays (see below). For these studies and for gene expression analyses, we used cycling cells, as they were clearly less sensitive to the polyQ expansion compared to serum-starved NGF-treated cells (Fig. 7). There was no evidence of any deficit in mitochondrial enzyme or aconitase activity in the HD-Q74 lines after 18 h of induction, compared with the same lines in the uninduced state, or HD-Q23 lines in the uninduced state (Table 2.). In a pilot experiment, we found no obvious mitochondrial compromise in an HD-Q74 cell line after 72 h of induction, compared with the same line in the uninduced state or an uninduced HD-Q23 line (data not shown). Cell death was not detectably increased in the HD-Q74 lines versus the HD-Q23 lines induced for <24 h (<2% cells with abnormal nuclei in either HD-Q23 or HD-Q74) (Fig 7A). Inclusions were found in 13% [± 5.2% (SD)] of HD-Q74 cells after 18 h induction.

Gene expression analyses

In order to measure expression changes in a wide range of genes, we have assayed changes in gene expression using Affymetrix arrays, Clontech filters and adapter-tagged competitive-PCR (ATAC-PCR) (see Materials and Methods for experimental details). These different approaches interrogated gene sets with minimal overlap. The Affymetrix arrays assayed approximately 7000 genes, the ATAC-PCR approximately 1000 genes and the Clontech Filters approximately 2400 genes. We used the Affymetrix U34A Rat Genome array, which includes genes encoding metabolic enzymes, growth factors and receptors, kinases and phosphatases, nuclear

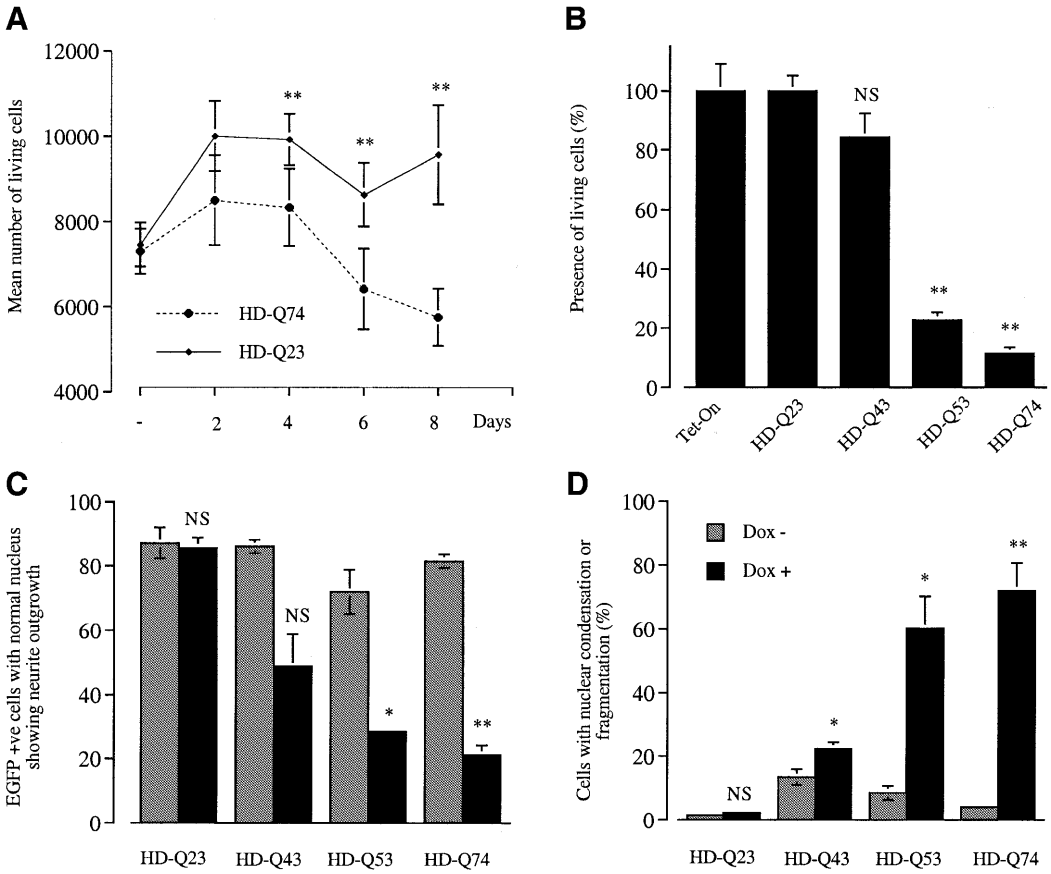

Figure 7. Cell death is increased in post-mitotic PC12 cells and the polyQ expansion inhibits neurite outgrowth in a polyQ length-dependent manner. (**A**) Cell loss for cycling PC12 HD-Q74 cells compared with HD-Q23 cells after transgene induction. Cells were seeded at equal densities and grown for 8 days and were either not treated or treated with 1 μg/ml dox for 2, 4, 6 or 8 days, after which time PI staining was performed and the number of living cells estimated using flow cytometry. Living cells were gated according to PI exclusion, size and granularity (Materials and Methods). Values are means of one representative triplicate experiment with SEM. $^{**}P < 0.001$ comparing HD-Q74 and HD-Q23 at a given time point (two-tailed *t*-test, unpaired). (**B**) Cell loss of post-mitotic PC12 HD-Q23, -Q43, -Q53, -Q74 and parental Tet-On cell line after transgene induction. Cells were seeded at equal densities and grown for 6 days in the presence of NGF and low serum conditions. Cells were either not treated or treated with 1 μg/ml of dox. Living cells were counted (haemocytometer) and dead cells excluded by trypan blue staining and expressed as ratios between cells present after dox treatment versus no treatment for each cell line. Mean values of one representative experiment performed in triplicate are shown with standard errors. $^{**}P < 0.001$ in comparison with HD-Q23 (two-tailed *t*-test, unpaired). (**C**) PolyQ length-dependent inhibition of neurite outgrowth. Post-mitotic EGFP-positive HD-Q23, -Q43, -Q53, -Q74 PC12 cells with normal nuclear morphology and cell shape showing one or more neurites (with length of at least one cell body diameter or more) were scored after no treatment or treatment with 1 μg/ml of dox for 6 days. Values represent means of two to three independent experiments with SEM. Asterisks, comparison of cells not treated with dox (Dox–, grey columns) versus cells treated with dox (Dox+, black colums). Legend as in (D). $^{*}P < 0.05$; $^{**}P < 0.001$ (two-tailed *t*-test, unpaired). (**D**) PolyQ length-dependent nuclear abnomalities after transgene induction in post-mitotic HD-Q43, -Q53, -Q74 cells. PC12 cells were grown on coverslips in the presence of NGF and low serum conditions and either untreated or treated with 1 μg/ml of dox for 7 days. Columns represent the proportions of EGFP-positive cells with a condensed or fragmented nucleus visualized by DAPI staining under a fluorescence microscope. Mean values of two to three independent experiments with SEM are shown. Statistics and comparison as in (C).

receptors, transcription factors, DNA damage repair proteins, apoptosis proteins, stress response proteins, membrane proteins and cell cycle regulators. This array also includes all of the genes found on the Affymetrix Rat Neurobiology U34 array. We assayed changes in expression after 18 h induction (Table 3). As a positive control in the ATAC-PCR experiments we determined expression levels of the HD-Q23 and -Q74 transgene mRNAs. In the uninduced state, the expression was 3.7, 2.2, 3.7 and 3.3 a.u. for HD-Q23 clonal lines 20 and 14, and HD-Q74 lines 10 and 1b, respectively. After 18 h induction the corresponding expression levels rose to 15.0, 21.5, 16.42 and 21.9 a.u. Fifty-six genes showed significant changes in mRNA expression (Table 3 and Materials and Methods). These include candidates that may be relevant to HD, including genes involved in apoptosis and metabolic regulation (Discussion). Five of the 56 genes showing early changes were transcription factors (ID1, ID2, c-erb, TSC-22 and BRIDGE).

cAMP response element (CRE)-mediated transcription is impaired in HD-Q74 cell lines

We have used the expression data as a preliminary starting point to build hypotheses regarding common pathways that may be perturbed by polyQ expansions. We searched the Medline database for promoter motifs present in the genes that showed altered expression in the HD-Q74 versus HD-Q23 lines at 18 h. Of the few genes that had some promoter characterization (less than 10), three had CREs and each of these was downregulated in the mutant cells: VGF8a, c-erbA α thyroid

Table 2. Mitochondrial function assays comparing three independent HD-Q74 cell lines in the uninduced state (HD-Q74–) versus the same three cell lines after 18 h induction (HD-Q74+) versus three independent HD-Q23 cell lines in the uninduced state (HD-Q23–)

	Citrate synthase	Complex I	Complex II/III	Complex IV	Aconitase
HD-Q23–					
Mean	926	0.082	0.220	0.019	20.9
SD	180	0.027	0.027	0.003	1.2
HD-Q74–					
Mean	844	0.104	0.270	0.019	17.3
SD	57	0.033	0.033	0.003	1.4
HD-Q74+					
Mean	771	0.094	0.314	0.020	18.5
SD	78	0.023	0.037	0.002	6.4

The means and SD values for the three independent lines are presented. The complex I, II/III and IV data are presented as the ratios of the relevant specific activities (nmol/min/mg)/CS specific activity, in order to correct for mitochondrial content. These ratios were determined for each cell line before determining the mean values presented in the Table.

hormone receptor and cathepsin L (31–33). We re-examined the gene array data of Luthi-Carter *et al.* (26) and noted down-regulation of 10/10 cAMP-responsive genes in HD transgenic mice versus controls. Thus, we tested if there was a generalized decrease in CRE-mediated transcription in the mutant cell lines. We made luciferase reporter constructs, where a wild-type or mutant CRE-binding protein (CREB)-binding site (that does not bind CREB) was inserted into the pGL3-promoter vector (Promega) that contains a minimal SV40 promoter. These vectors were transfected into either HD-Q23 or HD-Q74 lines with a plasmid containing the β-galactosidase gene driven by a constitutive human elongation factor 1α promoter, and β-galactosidase activity was quantified to control for transfection efficiency in each well. In each line we measured the difference between the wild-type and mutant CRE-containing vectors to determine the extent of promoter activity specifically due to CRE. We found that CRE-mediated transcription was significantly decreased in the HD-Q74 (clonal line 10) cells versus the HD-Q23 (clonal line 14) cells after 20 or 44 h induction (Fig. 9A). We subsequently confirmed this result in independent clonal lines expressing 74 and 23 repeats (Fig. 9B). We believe that β-galactosidase was a good transfection control, as its activity was not significantly different in uninduced versus induced cells (induced/uninduced β-galactosidase activities in HD-Q74 and HD-Q23 cells were 0.9 ± 0.1 and 1.0 ± 0.1, respectively).

cAMP stimulation partially rescues polyQ expansion-mediated cell death and impaired neurite outgrowth

In order to test whether decreased cAMP signalling contributed to the enhanced cell death and impaired neurite outgrowth seen in the HD-Q74 lines, we simultaneously treated PC12 cell lines with dox and NGF in low serum conditions and added either cAMP or forskolin, which activates adenylyl cyclase. Both cAMP and forskolin induced neurite outgrowth in the

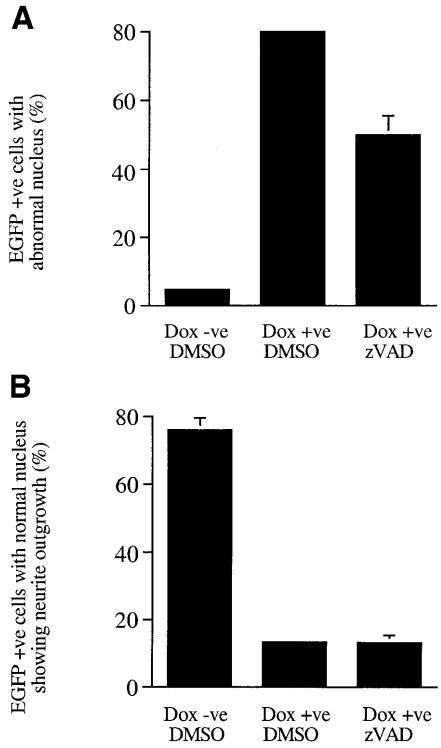

Figure 8. z-VAD-fmk reduces cell death in post-mitotic neurons (**A**) but does not improve neurite extension in healthy cells (**B**). HD-Q74 cells were seeded at equal densities and grown for 6 days in the presence of NGF and low serum conditions. Cells were either treated or not treated with 1 μg/ml of dox and the general caspase inhibitor zVAD-fmk (100 μM) or its carrier vehicle DMSO. In (A) columns represent the proportions of EGFP-positive cells with a condensed or fragmented nucleus visualized by DAPI staining under a fluorescence microscope. Mean values of two independent experiments in duplicate with SEM are shown. In (B) PC12 cells with normal nuclear morphology and cell shape showing one or more neurites (with length of at least one cell body diameter or more) were scored after no treatment or treatment with 1 μg/ml of dox for 7 days. Values represent means of two independent experiments in duplicate with SEM.

HD-Q74 cell lines (Fig. 10) and significantly reduced the proportions of cells with nuclear abnormalities, compared to untreated cells (Fig. 11). As expected (34), both cAMP and forskolin induced neurite outgrowth in the uninduced state (Fig. 10). In order to test whether this pathway was relevant to other neuronal and non-neuronal cells, we tested whether these compounds could reduce polyQ-induced cell death in transient transfection models using pEGFP-HDQ74 and pEGFP-HDQ103 constructs (20; Materials and Methods). We studied COS-7 (monkey kidney) cells and SK-N-SH (human neuroblastoma) cells, where these constructs caused significantly more cell death than pEGFP-HDQ23 or pEGFP-HDQ25 constructs (20). In both cell lines, polyQ-induced cell death was significantly reduced by either cAMP or forskolin compared to the DMSO vehicle control [SK-N-SH cells: cAMP versus DMSO, odds ratio (OR) = 0.27, 95% confidence interval (95% CI) = 0.17–0.44, $P < 0.0001$; SK-N-SH cells: forskolin versus DMSO, OR = 0.4, 95% CI = 0.27–0.6, $P < 0.0001$; COS-7 cells: cAMP versus DMSO, OR = 0.52, 95% CI = 0.35–0.75, $P < 0.001$; COS-7 cells: forskolin versus DMSO, OR = 0.6, 95%, CI = 0.41–0.90, $P < 0.05$; all experiments in triplicate wells performed twice. In all cases, we analysed the proportions of EGFP-expressing

Table 3. Gene expression changes in HD-Q74 lines versus HD-Q23 lines at 18 h after induction

Gene/function	Accession no.	Change	Gene/function	Accession no.	Change
Protein transport			Glucose/glycogen metabolism		
EST236721/cop-coated vesicle membrane protein p24 precursor	AI408431	↑* R	Insulin-like growth factor binding protein 5 protease	AF179370	↑* R
KIAAO719/Tom70 homologue	AJ243368	↑* R	Lipid/cholesterol metabolism		
Protein translation/ribosomal associated			Long-chain acyl-CoA synthetase/-CoA	D90109	↑* R
Ribosomal protein S7 (S8)	X53377	↑*C	ligase 2 (hs)		
Acidic ribosomal protein P0	Z29530	↓* R/↓* C	Long-chain acyl-CoA synthetase/-CoA	D10041	↑* R
Ribosomal protein S2	X57432	↑* R/↑ A	synthetase 5		
Protease function			Sulfated glycoprotein-prosaposin	U23740	↓* R
β proteasome subunit (Lmp3)	U65636	↓* R	EST215488 / VLDL receptor precursor	AI169603	↑* R
Cathepsin L	Y00697	↓* R	Novel protein expressed with nerve injury;	E12625	↓* A
RNA binding			RANP-1		
RNA-binding motif protein 3	AB016424	↓* R	Glycoprotein metabolism		
Transcriptional regulation			Arylsulfatase A	X73230	↑* R
Third largest RNA polymerase II subunit	D83999	↑* R	Iduronate-2-sulphatase gene	AA858833	↑* R
Transactivating protein BRIDGE	AF067728	↑* R	Nucleotide synthesis		
Retinoid binding			Equilibrative nitrobenzylthioinosine-sensitive	AB015304	↑* R
Retinol-binding protein (RBP) gene	K03045	↓* A	nuclear transporter		
Signalling pathways			Neurotransmission/Neuroexcitotoxicity/		
Cain	AF061947	↑* R/↑ A	CNS behaviour		
G protein γ 3 subunit (Gng3)	AF069953	↑* R	Serotonin 5-HT3 receptor	D49395	↓* A
KIAA0669; putative regulatory protein TSC-22	AB014569	↑* R	Homologous to human thymopoietin α = 87%	BE113158	↑* R
Alternative brain Ca^{2+}-ATPase	J04024	↑* R	EST207982/estrogen induced gene	AI013307	↑* R
Protein kinase associated			Mitochondrial function		
Protein kinase C (PKC) associated			Mitochondrial ATP synthase subunit 9,	U09813	↓* R
Protein kinase C Δ-binding protein	D85435	↑* A	P3 gene copy		
Perinuclear binding protein/PICK1	Z46720	↑* R	Homologous to ubiquinol-cytochrome c	AW525144	↑* R
Phosphatase			reductase core I protein (hs) = 89%		
ε isoform of 61 kDa regulatory subunit of PP2A	Z69029	↑* R	GAPDH	M17701	↓* C
Apoptosis			Cell adhesion		
ID1	D10862	↑* C	EST196658, 3′ end/rod outer segment protein	AA892855	↑* A
ID2	D10863	↑* C	C-CAM4/ectoATPase precursor	U23056	↓* A
RAC protein kinase α	D30040	↑* A/↑ C	Claudin-7	AJ011811	↑* A
c-erb-A thyroid hormone receptor	X12744	↓* A/↓ C	P-cadherin	D12688	↑* R
Cathepsin L	Y00697	↓* R	Target of the antiproliferative antibody; TAPA-1	U19894	↓* R
Cell death activator CIDE-B	AF061947	↑* R	Cytoskeletal organization		
Cell cycling/division/proliferation			C1-13 gene product	X52817	↓* A
Δ-like protein/zona glomerulosa-specific factor	D84336	↑* C/ ↑ A	Miscellaneous		
Cysteine-rich protein 2	D17512	↓* R/ ↓ A	UI-R-E0-ch-e-06-0-UI.s1, 3′ end/human	AA866432	↓* A
Opioid growth factor receptor	AI578564	↑* R	proteins KIAA0830		
Homologous to HRIHFB2007 (hs) = 84%	BE109521	↑* R	EST201485	AA945986	↑* R
Metabolism			EST222135	AI178461	↑* R
VGF8A protein precursor	M60525	↓* C	EST293018	AW142765	↑* R
Insulin-induced growth-response protein	L13619	↓* A	EST346357	AW915053	↑* R
(CL-6)			1-Tricarboxylate carrier-like protein	BE116904	↑* R

Upward arrows, genes upregulated in the HD-Q74 lines; downward arrows, genes that were downregulated in the HD-Q74 lines; asterisk, significant change; R, ATAC-PCR; C, Clontech filters; A, Affymetrix arrays. See Materials and Methods for experimental details. Note that the grouping of genes is somewhat arbitrary, since many genes have an impact on multiple pathways.

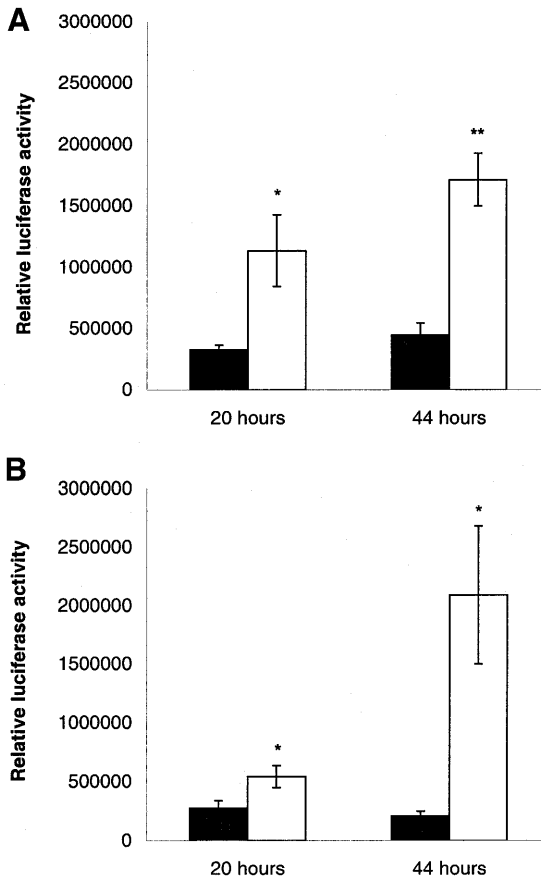

Figure 9. CRE-mediated transcription is impaired in HD-Q74 cell lines. Luciferase reporter assays were performed using inducible PC12 cells, and comparisons performed in two sets of different clonal lines. (**A**) Filled bar, HD-Q74 line10; empty bar, HD-Q23 line 14. (**B**) Filled bar, HD-Q74 line1b; empty bar, HD-Q23 line 7. Cells were induced with dox (1 μg/ml) 4 h after seeding for 20 or 44 h, as indicated on the *x*-axis. The luciferase activity from each well was normalized to the β-galactosidase to control for variations in transfection efficiency. The relative amount of luciferase activity specifically due to the presence of the CREB-binding site was obtained by subtracting the luciferase activity in cells expressing mutant pGL3-CREB from those expressing wild-type pGL3-CREB. Each promoter construct was transfected in three different experiments. The results represent the means of data from six or seven wells. Error bars indicate the SD. Significance was shown at the $P < 0.03$ (*) and $P < 0.001$ (**) levels.

cells with nuclear abnormalities after cAMP or forskolin treatment for 48 h after transfection; see Materials and Methods for description of ORs]. Neither forskolin nor cAMP significantly altered the proportions of EGFP-expressing cells with aggregates ($P > 0.05$ for all comparisons).

DISCUSSION

Our inducible PC12 cell lines recapitulate many of the features of HD seen *in vivo.* The polyQ expansion is associated with the formation of aggregates with an EM structure similar to that seen *in vivo* (18) and decreased neurite outgrowth. Our cell model allowed us to compare the effects of polyQ expansions in cycling versus post-mitotic cells from the same clonal origins, induced with the same dose of dox. In cycling cells, the aggregates first formed in the nucleus followed by a progressive increase in the proportion of cells with both nuclear and cytoplasmic aggregates (Fig. 3). However, in post-mitotic PC12 cells, aggregates formed in the nucleus, but not in the cytoplasm. This suggests that the nucleus may represent a preferential environment for aggregate formation. It seems that the proportion of cytoplasmic versus nuclear inclusions is enhanced by cell division. In dividing cells, aggregates may be dispersed during mitosis (35) and the breakdown of the nuclear membrane during cell division may allow aggregates that originally formed in the nucleus to move into the cytoplasm. The few post-mitotic cells in our cell model in which aggregates were found outside the nucleus may have divided after NGF exposure. As seen *in vivo*, the polyQ aggregates sequester ubiquitin, HSPs and proteasomal components (reviewed in 36). It is interesting that ubiquitin appeared to associate with inclusions at later time points. A similar phenomenon was recently reported in HD transgenic mice (21). Thus, ubiquitination may be a 'late' event, or epitopes may be hidden at earlier time points.

It is possible that the post-mitotic state of virtually all neurons is one of the reasons why the CNS is more susceptible to polyQ mutations than many other tissues expressing the mutant proteins. Expression of htt exon 1 containing a Q74 expansion (HD-Q74 PC12 cells) for 6 days resulted in a 10–20% loss of cycling cells, while significantly higher loss was seen in post-mitotic cells (up to 90%) (Fig. 6). Furthermore, the nuclear condensation and fragmentation observed in post-mitotic HD-Q74 cells was almost never detected in cycling HD-Q74 PC12 cells, indicating that polyQ toxicity was more severe in cells that did not divide. These findings are compatible with those of Yoshizawa *et al.* (37) for DRPLA.

Cell death in our lines was reduced by the general caspase inhibitor zVAD-fmk, but not the caspase-3-like inhibitor, zDEVD-fmk, as shown by Ona *et al.* (38) and Chen *et al.* (39) for HD transgenic mouse models, and Kim *et al.* (40) for an HD cell model. Thus, polyQ mutations may induce similar caspase-dependent death pathways in different cell types, involving more than caspase 3 alone.

The reduced neurite outgrowth seen in our cell lines may be a surrogate for the reduced number of dendrites seen in HD patients. Li *et al.* (41) showed that PC12 cells overexpressing htt exon 1 with 150 glutamines have defective neurite development. This could have been simply due to cell death; for instance, CREB, which plays an important role in neurite outgrowth, can be degraded by caspases (42). Our data suggest that this phenomenon is not simply a secondary consequence of cell death, as we observed a polyQ length-dependent impairment of neurite outgrowth in cells with normal nuclear morphology. Furthermore, unlike cell death in post-mitotic cells, we showed that neurite outgrowth was not rescued by zVAD-fmk. Thus, impaired neurite outgrowth in our PC12 model may be a sign of cell dysfunction that precedes cell death, similar to what is seen *in vivo* (10,11). However, the polyQ expansion mutation may perturb a common pathway affecting cell survival and neurite outgrowth, because the failure of neurite outgrowth and cell death were strongly correlated in the post-mitotic PC12 cells.

Our data suggest that the increased susceptibility to cell death and decreased neurite outgrowth are partly due to impaired CRE-transcriptional responses. The reduction in CRE-mediated transcription determined by reporter assays

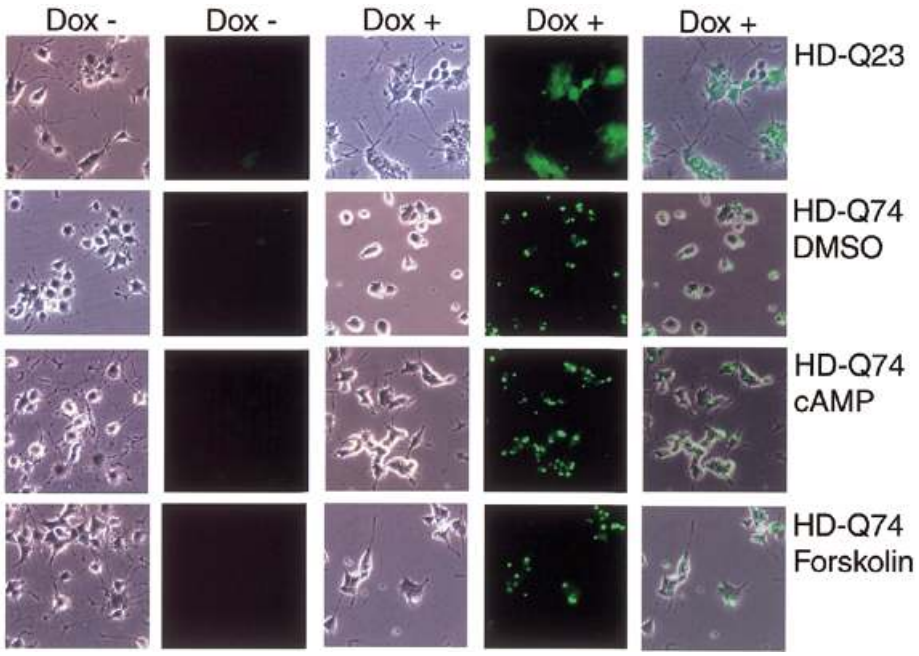

Figure 10. cAMP and forskolin partially rescue neurite outgrowth in serum-starved NGF-treated HD-Q74 cells. HD-Q23 and HD-Q74 cells were seeded at equal densities and grown for 5 days in the presence of NGF and low serum conditions in the presence of DMSO (carrier), forskolin (20 μM) or cAMP (800 μM) in the presence or absence of dox. Dox, forskolin, cAMP or DMSO were added every 24 h when medium was replaced. While there was significantly more cell death in the untreated HD-Q74 dox+ cells, we have specifically chosen a field with abnormally high cell density to allow visualization of an appropriate number of cells to assess the degree of neurite outgrowth.

was consistent with the downregulation of the three genes with CRE elements in their promoters that showed significant changes in our gene expression analyses. A reduction of CRE-mediated transcription is also likely in human HD, since reduced levels of the CRE-responsive genes, somatostatin, corticotrophin releasing hormone, proenkephalin and substance P, are seen in HD versus control brains, even in early stages of the disease (43–46). This pathway is also likely to be impaired in mouse models, since 10/10 cAMP responsive genes showing changes in HD mice were downregulated (26).

Our reporter gene assays, which measured the ability of the PC12 cells to activate a CRE promoter construct, complement those previously performed that suggested that the cells expressing expanded polyQs had an impaired ability to activate a transfected CREB construct (47). While we were writing this manuscript, Nucifora *et al.* (48) reported decreased CRE-mediated transcription in their HD models. Since CRE-mediated transcription appears to be impaired in three different polyQ disease models (HD, DRPLA and SBMA), it will be important to test if this is one of the unifying features common to all polyQ diseases (47–49).

Decreased expression of CRE-responsive genes appears to be relevant to the cellular pathology of our HD model, since polyQ-induced cell death and impaired neurite outgrowth in post-mitotic PC12 cells were rescued by cAMP and forskolin [which lead to phosphorylation and activation of CREB via protein kinase A (34)]. cAMP and forskolin also reduced polyQ-induced cell death in non-neuronal COS-7 and neuronal SK-N-SH cells. Thus, decreased CRE signalling may be a generic cellular consequence of polyQ mutations. These effects are likely to be due to CRE signalling rather than other effects resulting from cAMP modulation, since CRE-transcriptional responses are known to modulate cell death and neurite outgrowth in PC12 cells (34). Furthermore, PC12 differentiation can be mediated directly via overexpression of phosphorylated CREB (34). While previous studies have suggested that polyQ-induced cell death can be attenuated by overexpression of CREB-binding protein (CBP) or $TAF_{II}130$ (47–49), which can both activate CREB-mediated transcription, these co-activators also interact with a wide variety of other transcription factors and CBP directly acetylates nucleosomes (50,51). Thus, the protective effects of CBP and $TAF_{II}130$ on polyQ toxicity could have been independent of CRE pathways. However, our findings of protective effects of cAMP and forskolin complement these previous studies and strongly implicate disruption of CRE-mediated transcription in polyQ disease pathogenesis. Our data suggest that this pathway is also important in relation to neurite outgrowth, which may impact on cell dysfunction that occurs in the early stages of polyQ diseases prior to cell death (10). Indeed, decreased CRE-mediated transcription occurred in our mutant cell lines before overt cell death, mitochondrial compromise and a large inclusion load. This may be relevant *in vivo*, since CREB-mediated signalling is crucial for long-term potentiation (LTP), the synaptic analogue for memory (52). LTP is impaired in a number of HD mouse models and memory difficulties are a feature of HD (53,54).

There are a number of potential non-mutually exclusive mechanisms that may act upstream of CREB in polyQ diseases. Decreased adenylyl cyclase activity has been observed in HD transgenic mice (26). It is possible that some of these changes may be mediated by the increased levels of

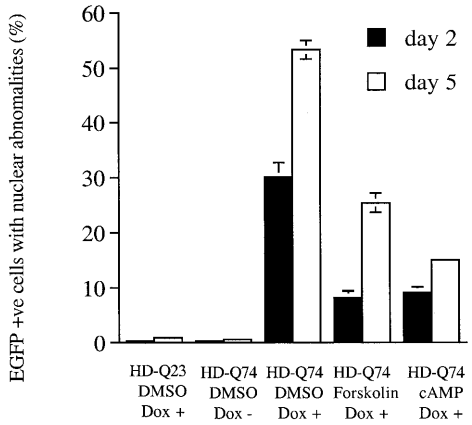

Figure 11. cAMP and forskolin partially rescue cell death in serum-starved NGF-treated HD-Q74 cells. HD-Q23 and HD-Q74 cells were seeded at equal densities and grown for 2 or 5 days in the presence of NGF and low serum conditions in the presence of DMSO (carrier), forskolin (20 μM) or cAMP (800 μM) in the presence or absence of dox. Dox, forskolin, cAMP or DMSO were added every 24 h when medium was replaced. This experiment was performed twice in triplicate. Data from one experiment are shown. The pooled analysis for both experiments was as follows for cAMP versus DMSO in dox+ HD-Q74 cells: day 2, OR = 0.15, 95% CI = 0.11–0.20 , $P < 0.0001$; day 5, OR = 0.15, 95% CI = 0.11–0.22, $P < 0.0001$. For forskolin versus DMSO in dox+ HD-Q74 cells: day 2, OR = 0.18, 95% CI = 0.14–0.25, $P < 0.0001$; day 5, OR = 0.32, 95% CI = 0.24–0.43, $P < 0.0001$.

protein phosphatase 2A suggested by our expression assays. This enzyme is a major phosphatase that deactivates phosphorylated CREB (55), one of the main transcription factors that bind to CRE elements. Another appealing model invokes the sequestration of coactivators like CBP and $TAF_{II}130$ by mutant polyQ stretches into inclusions, as these co-activators are important positive regulators of CREB-mediated transcription. CBP has been observed in aggregates in SBMA (49), HD and DRPLA (56,48) and $TAF_{II}130$ in SCA3 and DRPLA (47). It may be difficult to unravel the relative importance of these different mechanisms.

In addition to the decreased CRE-mediated transcription seen in our model, there are other transcriptional changes that are interesting and may merit robust confirmation in future studies (particularly where we have not used RT–PCR). Some of the mRNA expression changes we observed have parallels in human HD and in mouse models. For instance, we found downregulation of the 5-HT3 serotonin receptor and recognition sites for this receptor are decreased in human HD striatum (57). Confirmation of this change would suggest this gene as a candidate for the depressive symptoms seen in HD. Like Luthi-Carter *et al.* (26) we observed decreased expression of retinol-binding protein, consistent with their suggestion of decreased transcriptional activation via retinoid receptors. VGF8a appeared to be downregulated in our HD-Q74 cells, possibly because it is CRE-regulated. If this change is confirmed in *in vivo* studies, then this may be a candidate that would explain the cachexic symptoms of HD. Studies in VGF knockout mice suggest that it has an important role in energy homeostasis and these mice are thin, small, hyperactive and hypermetabolic (reviewed in 58).

It was noticeable that a large number of the genes that showed alterations in our screen were transcription factors (ID1, ID2, c-erb, TSC-22 and BRIDGE), which may represent some of the early changes occurring in the disease. The ID1 and ID2 may be important for follow-up studies, since these are dominant-negative regulators of basic helix–loop–helix proteins, and ID overexpression can be pro-apoptotic and inhibit neuronal differentiation (59,60).

In conclusion, polyQ-mediated cell death in tissue culture models is caspase-dependent, and requires more than caspase 3, as observed in mouse models. Cell death is increased in post-mitotic cells, which may explain part of the neuronal vulnerability to polyQ mutations. At early times after transgene induction, before cells expressing mutant constructs have a high inclusion load, mitochondrial dysfunction or increased cell death, we observed a decrease in CRE-mediated transcription. This was compatible with changes in mRNA expression patterns noted by ourselves in cell models and by others in animals models and in the human disease. This pathway deserves serious consideration as it impacts on cell death, neurite outgrowth and other functions like LTP, and appears to be similarly affected in at least three polyQ diseases.

MATERIALS AND METHODS

Plasmid construction and establishment of inducible PC12 cell lines

Genomic DNA from individuals with 21, 41, 51 or 72 CAG repeats was used as a template for amplifying codons 8–57 inclusive of exon 1 of the HD gene (numbering applies to htt with 23 Q residues which is equivalent to 21 uninterrupted CAG repeats) following a strategy described previously (20). PCR products were ligated into the *Bgl*II and *Eco*RI restriction sites of EGFP-C1 (Clontech, Basingstoke, UK). These plasmids were digested with *Eco*47III and *Eco*RI to release exon 1 containing 21, 41, 51 or 72 CAG repeats tagged to EGFP, which was religated into the *Eco*RI and blunt-ended *Sac*II sites of pTRE (Clontech). pTRE constructs were co-electroporated with pTK-Hyg (Clontech) into PC12 Tet-On cells (Clontech) using a 10:1 excess of pTRE to allow selection of stably transformed cells in the presence of hygromycin (150 μg/ml). Single cell-derived colonies for each polyQ construct were isolated by ring cloning. Cells were then maintained at 75 μg/ml hygromycin in standard medium consisting of high glucose DMEM (Sigma, Dorset, UK and Upstate Biotechnology, NY) with 100 U/ml penicillin/streptomycin, 2 mM L-glutamine (Life Technologies, Paisley, UK), 10% heat-inactivated horse serum (HS) (Life Technologies), 5% Tet-approved fetal bovine serum (FBS) (Clontech) and 100 μg/ml G418 (Life Technologies) at 37°C, 10% CO_2.

Characterization of inducible PC12 cell lines

Dose–response/expression level experiments. Equal numbers of cells were seeded into six-well plates, grown for 48 h and subsequently left uninduced or induced for 8 h using dox at indicated doses. After trypsinization, single cell suspensions were analysed by flow cytometry (20 000 cells analysed).

PolyQ length- and time-dependent aggregation

Cells were seeded on coverslips in standard medium and after 24 h were induced using dox (1 μg/ml) for the indicated times,

washed, fixed and mounted (see below). 500–1000 EGFP-positive cells were analysed per coverslip. PolyQ aggregation in post-mitotic PC12 cells was estimated by treating cells with NGF and low serum media (see below) for 6 days, after which cells were induced with dox. Nuclear localization of inclusions was considered positive if the EGFP inclusions were totally surrounded by the DNA dye 4′,6-diamino-2-phenylindole (DAPI) (100–200 EGFP-positive cells/coverslip).

Treatment with NGF

For co-localization studies (see below), cells were seeded on coverslips and 24 h later exposed to 100 ng/ml of NGF (Sigma) under low-serum conditions (1% HS) for 6 consecutive days and induced subsequently using 1 μg/ml of dox. For cell death and neurite outgrowth experiments, cells of similar passage number were either induced or left uninduced for 24 h (1 μg/ml dox) after which the cells were seeded at $1–2 \times 10^5$ per well on coverslips in NGF/1% HS. Coverslips were coated with Collagen Type I (1 mg/ml) (Sigma), air dried and overlaid for 1 h with DMEM containing rat laminin (10 μg/ml) (Life Technologies).

FACS analysis

Quantitative flow cytometry was performed as described previously (20). For some experiments (see below), cells were exposed to propidium iodide (PI) at 1 μg/ml in 1× PBS for 10 min.

Immunocytochemistry and western blotting

For co-localization studies, PC12 HD-Q23, -Q43 and -Q74 cells were grown on coverslips coated with poly-ornithine (10 μg/ml in DMEM, overlay for 1 h), left uninduced or treated with dox (1000 ng/ml) for either 1–2, 3–4 or 6–7 days. For studies of NGF-differentiated PC12 cells, coverslips were additionally coated with rat laminin (see above). Immunocytochemistry was performed as described previously (20). Antibodies were rabbit anti-HDJ-1 polyclonal/1:1000 (SPA-400, Stressgene, Victoria, CA), mouse anti-HDJ-2 monoclonal/1:200 (Neomarker, Fremont, CA), rabbit anti-HSP25 polyclonal/1:200 (Stressgene), mouse anti-HSP27/1:400 (Neomarker), mouse anti-HSP70 monoclonal/1:200 (SPA-810, Stressgene), rat anti-HSC70 monoclonal/1:400 (Stressgene), mouse anti-HSP90 monoclonal/1:200 (Stressgene), rabbit anti-HSP110 polyclonal/1:200 (Stressgene), mouse anti-ubiquitin monoclonal/1:200 (Chemicon, Harrow, UK), rabbit anti-11S proteasome regulator subunit PA28 (α, β and γ) polyclonal/1:2000 (Affiniti, Exeter, UK), rabbit anti-19S regulator ATPase subunit 8 (p45) polyclonal/1:200 (Affiniti), rabbit anti-20S proteasome polyclonal/1:200 (Affiniti) and rabbit anti-ubiquitin conjugating enzyme E2 polyclonal/1:200 (Affiniti).

For western blotting, cell pellets were lysed in 1% Triton X-100, 150 mM NaCl, 25 mM Tris–HCl and 0.4% SDS for 30 min on ice in the presence of protease inhibitors (Roche, Lewes, UK), centrifuged at high speed for 20 min at 4°C and supernatants subjected to SDS–PAGE (12%). Antibodies were mouse anti-GFP monoclonal (1:1000, Clontech) and rabbit anti-actin polyclonal (1:2500, Sigma). Blots were probed with peroxidase-labelled anti-mouse or -rabbit antibodies at 1:2500 (Amersham, Buckinghamshire, UK). Bands were visualized with the ECL detection reagent (Amersham).

Preparation of EM samples

Aliquots of 25 cm^2 (80% confluency) of untreated and dox-treated (48 h) PC12 HD-Q23 and -Q74 cells were pelleted, fixed overnight in 2% paraformaldehyde/2.5% glutaraldehyde in 0.1 M Na-cacodylate-HCl buffer (pH 7.2), washed and postfixed in 2% osmium tetroxide for 1 h. Then, cell pellets were treated with 50:50 epoxy-propane:araldite CY212 resin overnight and finally embedded in fresh resin and cured for 2 days at 60°C. Sections (70 nm) were cut on a ultracut microtome (Leica), mounted on grids, stained with 7.5% uranylacetate in methanol for 30 s and analysed by EM (100CX/TEM, Philips).

Cell death assays, caspase inhibition and estimation of neurite outgrowth

Presence and absence of living cells. We seeded an equal number of HD-Q23 and -Q74 cells and either left these uninduced or induced for 2, 4, 6 or 8 days. Cells in each dish were then resuspended in equal volumes of 1× PBS to get single cell suspensions and each suspension was analysed by flow cytometry for a constant time period (1 min). Living cells were identified by PI exclusion, size and granularity. This experiment was performed in triplicate. To estimate the presence of living cells after induction of htt exon 1 in post-mitotic cells, we seeded HD-Q23, -Q43, -Q53, -Q74 and parental Tet-On cells into six-well plates, grew these for 3 days, primed cells with NGF (100 ng/ml) and induced with dox (1 μg/ml) simultaneously for 24 h or left cells uninduced in parallel dishes. Then, cells were re-seeded at equal numbers ($1–2 \times 10^5$ per well) in six-well plates. Plates were coated with Collagen Type I (1 mg/ml) and rat laminin (10 μg/ml) (see above). Cells were then treated for 6 days with/without dox (1 μg/ml) and NGF/1% HS (see above), washed twice, treated with trypsin and resuspended in equal volumes of 1× PBS with addition of 0.4% trypan-blue (1:100). The numbers of living (trypan-blue-excluding) cells in each dish were estimated using a haemocytometer (two experiments in triplicate; means obtained from five to ten counting events per well).

Nuclear morphology and TUNEL assay

The morphology DAPI-stained nuclei was considered abnormal if the nucleus was fragmented or condensed to a small size. We analysed 100–200 EGFP-positive COS-7 or SK-N-SH cells per coverslip and 50–200 PC12 inducible cells. Cells exhibiting DNA strand breaks were detected by TUNEL using 3,3′-diaminobenzidine as a chromogenic substrate (Roche). For time-course experiments using HD-Q23, -Q43, -Q53 and -Q74 cells, we counted TUNEL positive cells in 5–10 randomly chosen visual fields of similar density (80%) in two to three independent experiments. To estimate the proportion of TUNEL-positive cells for the HD-Q74 clonal line, we counted at least 1000 cells.

Caspase inhibition

zVAD-fmk (100 μM) and zDEVD-fmk (200 μM) (Calbiochem, Nottingham, UK) were added to the media every 24 h.

Neurite outgrowth

PC12 cells that exhibited one or several neurites, which were equal to or exceeded the diameter of the cells body in length, were scored as positive. We performed two to three independent experiments using single standing cells from independent clonal lines with similar passage numbers. We counted 50–200 cells and only considered cells with normal nuclear morphology.

cAMP and forskolin treatments

Cells were grown for the indicated periods in the presence of DMSO (carrier), forskolin (20 μM), or cAMP [8-(4-chlorophenylthio)adenosine3′:5′-cyclic monophosphate] (800 μM) (Sigma). PC12 cells were grown in NGF/1% HS. In transient expression experiments in COS-7 (monkey kidney) cell lines, we used HD gene exon 1 fused to EGFP containing 74 glutamine repeats (pEGFP-HDQ74) (EGFP at N-terminus, EGFP-C1; Clontech) and a comparable construct with 23 glutamines. In SK-N-SH (human neuroblastoma) cells, we used a construct expressing HD gene exon 1 fused to EGFP with 103 repeats (pEGFP-HDQ103) (EGFP at C-terminus, EGFP-N1; Clontech), and a comparable construct with 25 glutamines, kind gifts from Drs A.Tobin and G.Lawless. These constructs were transfected and analysed as described previously (20).

Statistical analysis

Pooled estimates for the changes in inclusion formation/cell death resulting from experimental manipulations assessed in multiple experiments were calculated as ORs with 95% CIs (20). ORs compare the proportions of EGFP-expressing cells with or without inclusions (or nuclear abnomalities) under perturbed conditions (e.g. cAMP treatment), to proportions observed under control conditions (e.g. DMSO carrier control in cAMP experiments). ORs and *P*-values were determined by unconditional logistical regression analysis by using the general loglinear option of SPSS 9.0.1 software (SPSS, Chicago). For some experiments we applied *t*-tests (two-tailed) or linear regression analysis (Statview for Windows, Version 4.5, Chicago).

Mitochondrial function assays

For each cell line, samples were harvested from ten 10 cm diameter plates (80–90% confluent) as described (61), with the exception that the homogenization buffer was 10 mM Tris–HCl pH 7.4/0.25 M sucrose/1 mM EDTA. Following three freeze–thaw cycles, mitochondrial complex I (rotenone-sensitive NADH CoQ_1 reductase), complex II/III (succinate cytochrome c reductase), complex IV (cytochrome oxidase) and citrate synthase (CS) activities were assayed at 30°C as described (62). Aconitase activity was analysed as described previously (63). Protein concentrations were determined by the procedure of Lowry *et al*. (64) using bovine serum albumin as a standard. Specific enzyme activities are expressed in nmol/min/mg. Mitochondrial respiratory chain activities are also expressed as a ratio with CS.

mRNA expression analyses

mRNA extraction. Total RNA was extracted from three different clonal lines of HD-Q74 and HD-Q23 after 18 h induction with 1 μg/ml dox. Six millilitres of TRIzol™ reagent (Life Technologies) was added to each 75 cm^2 flask at 80% confluency and the RNA was extracted using the manufacturer's protocol. RNA samples were resuspended in RNAse-free water and quantified spectrophotometrically. The integrity of all samples was confirmed by gel electrophoresis, demonstrating a 2-fold excess of 28S to 18S RNA, with no evidence of degradation.

ATAC-PCR. Two 3′-directed cDNA libraries were constructed using RNAs from the uninduced HD-Q23 (line 20) and HD-Q74 (line 10) cells induced with dox for 20 h, as described previously (65). A total of 4006 unique EST sequences was obtained from single pass sequencing of 12476 cDNA clones. We selected 1824 genes for primer design, prioritizing known genes and abundant unknown genes. ATAC-PCR reactions were performed as described previously (66). However, seven adaptors were used, instead of six in the previously described method. Three adaptors were assigned for control cDNAs, which were made from RNA of the 21.10 cell line. Four adaptors were assigned for the sample cDNAs. Each sample was assayed twice with different calibration. One calibration used 10×, 3× and 1× equivalents of the control sample compared to a 1× equivalent of the test sample. The other calibration used 1×, 3× and 10× equivalents of the control sample compared to a 3× equivalent of the test sample. Relative expression levels were calculated using calibration curves based on the control samples. Good quality data were obtained from 1049 genes.

Affymetrix. Twelve micrograms total RNA were used as the starting material for the cDNA preparation. The first and second strand cDNA synthesis was performed using the SuperScript Choice System (Life Technologies) according to the manufacturer's instructions except using an oligo(dT) primer containing a T7 RNA polymerase promoter site. Labelled cRNA was prepared using the MEGAscript *in vitro* Transcription (IVT) kit (Ambion). Biotin-labelled CTP and UTP (Enzo) were used in the reaction together with unlabelled NTPs. Following the IVT reaction, the unincorporated nucleotides were removed using RNeasy columns (Qiagen). Fifteen micrograms of cRNA were fragmented at 94°C for 35 min in a fragmentation buffer containing 40 mM Tris-acetate pH 8.1, 100 mM KOAc, 30 mM MgOAc. Prior to hybridization, the fragmented cRNA in a 6× SSPE-T hybridization buffer (1 M NaCl, 10 mM Tris pH 7.6, 0.005% Triton) was heated to 95°C for 5 min and subsequently to 40°C for 5 min, before loading onto the Affymetrix probe array cartridge. The probe array was then incubated for 16 h at 40°C at constant rotation (60 r.p.m.). The washing and staining procedure was performed in the Affymetrix Fluidics Station. The probe array was exposed to 10 washes in 6× SSPE-T at 25°C followed by four washes in 0.5× SSPE-T at 50°C. The biotinylated cRNA was stained with a streptavidin–phycoerythrin conjugate, 10 mg/ml (Molecular Probes, Eugene, OR), in 6× SSPE-T for 30 min at 25°C followed by 10 washes in 6× SSPE-T at 25°C. The probe arrays were scanned at 560 nm using a confocal laser-scanning microscope with an argon ion laser as the excitation source

(Hewlett Packard GeneArray Scanner G2500A). The readings from the quantitative scanning were analysed by the Affymetrix Gene Expression Analysis Software. For comparison from array to array, these were scaled to a global intensity of 150, as published previously (67).

cDNA microarray screening

^{32}P-labelled cDNA was prepared using [α-^{32}P]dATP from 3 μg total RNA derived from two clonal cell lines, namely HD-Q74 line 10 versus HD-Q23 line 20, or HD-Q74 line 1b versus HD-Q23 line 14. RNA was hybridized to the Atlas Rat cDNA Expression Array, 588 genes (catalogue number 7738–1; Clontech Laboratories, Palo Alto, CA); Atlas Rat Stress/Toxicology Array, 207 genes (catalogue number 7735–1; Clontech); Atlas Rat Toxicology Array II, 465 genes (catalogue number 7732–1; Clontech) and the Atlas Rat 1.2 Array II, 1176 genes (catalogue number 7856–1; Clontech) according to the user manual. Expression was visualized by exposing filters to a phosphor screen and analysed with a Packard Cyclone Storage Phosphor System. Spot alignment and intensity was quantified using the AtlasImage 1.5 software package (Clontech). Global sum normalization mode was selected to calculate the overall normalization coefficient when comparing arrays. The ratio and difference thresholds used were the default values adopted by the program software.

Selection criteria for genes showing significant changes

For the Clontech microexpression array analysis, significant gene changes between the two comparative samples were those in which the ratio threshold was ≥2 (for upregulated genes) or ≤0.5 (for downregulated genes). Only those genes that showed such changes in one HD-Q74 versus one HD-Q23 line that met the same criteria and changed in the same direction in an independent set of HD-Q74 and HD-Q23 lines, were deemed to be significantly changed.

With the Affymetrix gene chips, significant gene changes in any comparison were limited to fold changes of three or more, where the sort score was ≥0.5. The sort score is a function of both the fold change and average difference change between samples. It can be used to evaluate the 'significance'/reliability of the differences observed. Each sample comprised a pool of equal amounts of mRNA from three different clonal lines of HD-Q74 or -Q23 induced for 18 h or left uninduced for 18 h. Since single chips were run for the normal and expanded repeat pools in different induced and uninduced conditions, we only selected genes where there were changes in the same direction in two different comparisons. First, we selected changes that were consistent when comparing HD-Q74 cells induced for 18 h to HD-Q23 induced for 18 h, where the HD-Q74 induced sample also showed a significant change in the same direction when compared to uninduced HD-Q74 cells. A second group of genes was selected which showed similar significant differences between HD-Q74 and HD-Q23 clonal lines induced for 18 h, as between HD-Q74 uninduced versus HD-Q23 uninduced. Since uninduced cells have low background transgene expression, we felt that this set reflected genes which show differences in HD-Q23 and -Q74 at both high and low transgene expression levels. For all comparisons we excluded genes that showed significant changes in HD-Q23 in the induced versus the uninduced state.

For ATAC-PCR, genes showing a 2-fold increase or decrease in expression after 18 h induction compared with the uninduced state in two independent 72 repeat cell lines, but not in two independent 21 cell lines, were selected for further consideration. From this set of genes, we selected those that showed at least 2-fold differences in expression at the 18 h point when comparing the two independent 72 repeat lines with the two independent 21 repeat lines.

Cross comparisons between the three different methods were made, where genes were common to two or more techniques. We have discarded Affymetrix data with sort scores of 0.05 or less for these comparisons, as these are too unreliable given the very low number of hybridizing oligonucleotides in the gene. Of the six Clontech genes meeting cut-off criteria for significance, two had sort scores of >0.05 on the Affymetrix system. Of these significant Clontech changes, one (delta-like protein) showed a non-significant change in the same direction in the Affymetrix system. While GAPDH showed a significant change in the Clontech filters it had no change in the Affymetrix system. Twelve genes met the criteria for significance on the Affymetrix arrays, of which two were represented on the Clontech membranes. In both these cases (c-erb-A thyroid hormone receptor and RAC protein kinase α) the changes seen in the Clontech system were in the same direction as on the Affymetrix arrays.

Using the ATAC-PCR analysis, 44 genes met the criteria for significance. However, five of these were excluded from final tabulation as they were represented in two or three of the experimental systems and changes seen were inconsistent in direction. Of the remaining 39 genes, two were also represented on the Affymetrix system with the sort score being ≥0.05. In both cases (cain and ribosomal protein S2), the changes on the Affymetrix arrays are consistent with the ATAC-PCR data. Another one gene was represented on the Clontech membranes, where the change was in the same direction and significant (acidic ribosomal protein P0), as shown in the table.

Luciferase assays

Promoter constructs. The promoter element which binds CREB wild-type (CREB-wt) (Geneka catalogue, Canada), or a mutated promoter element which does not bind CREB mutant (CREB-mt) (Geneka) were incorporated into oligonucleotides with a 5′ *Sac*I site, a *Pst*I unique linker site and a 3′ *Nhe*I site, when in double-stranded form. The forward sequences of these oligonucleotides were as follows: CREB-wt consensus sequence 5′-CCTGCAGGATTCAATGACATCACGGCTG-TGG-3′ and CREB-mt consensus sequence 5′-CCTGCAGGA-TTCAAGAACATAGCGGCTGTGG-3′. These were double-digested, purified and ligated into identical sites in the pGL3-promoter luciferase vector (Promega, Southampton, UK), containing the SV40 promoter.

DNA transfections, luciferase and β-galactosidase assays. Two clonal lines of stably transfected PC12 HD-Q74 (lines 10 and 1b) and PC12 HD-Q23 (lines 14 and 7), were transfected using LipoFECTAMINE PLUS™ Reagent (Gibco BRL, Life Technologies, UK). Luciferase reporter assays were performed as described (68). We co-transfected 750 ng of plasmid

containing CREB-wt or CREB-mt, with 300 ng of a plasmid containing the gene for β-galactosidase linked to a constitutively active human elongation factor 1α promoter, into cells in a 24-well plate. Cells were induced with 1 μg/ml dox 4 h thereafter and then harvested either 24 or 48 h after transfection. The luciferase activity from each well was normalized to the β-galactosidase to control for variations in transfection efficiency. To measure the amount of luciferase activity specifically due to the presence of the CREB-binding site we subtracted the luciferase activity in cells expressing mutant pGL3-CREB from those expressing wild-type pGL3-CREB.

ACKNOWLEDGEMENTS

We thank L.Ho for help with analyses of some caspase experiments, Y.Narain for help with EM analysis, A.Tobin and G.Lawless for providing constructs and J.Arthur for assistance with fluorescent microscopy. We are grateful to the Hereditary Disease foundation (A.W. and D.C.R.), The Swiss National Science Foundation (A.W.), Merck Sharp and Dohme (A.W. and J.S.), Action Research (J.C.), The Violet Richards Charity (D.C.R.), The Isaac Newton Trust (D.C.R.), Core Research for Evolutional Science and Technology, Japan Science and Technology Corporation (K.K.), Ataxia (J.B. and A.S.) and the National Lottery (J.B. and A.S.) for financial support. J.S. and J.C. are grateful for Sackler studentships. D.C.R. is a Glaxo Wellcome Research Fellow.

REFERENCES

1. Huntington's Disease Collaborative Research Group (1993) A novel gene containing a trinucleotide repeat that is expanded and unstable on Huntington's disease chromosomes. *Cell*, **72**, 971–983.
2. Ross, C.A. (1997) Intranuclear neuronal inclusions: a common pathogenic mechanism for glutamine-repeat neurodegenerative diseases? *Neuron*, **19**, 1147–1150.
3. Nakamura, K., Jeong, S.Y., Ichikawa, Y., Nagamisha, K., Nagamisha, T., Goto, J., Ikeda, S. and Kanazawa, I. (2000) SCA13, a novel autosomal dominant cerebellar ataxia caused by the expanded polyglutamine in TATA-binding protein identified with IC2 antibody immunoscreening. *Am. J. Hum. Genet.*, **67** (Suppl. 2), 389.
4. Margolis, R.L., O' Hearn, E., Rosenblatt, A., Troncoso, J., Holmes, S., Franz, M.L., Sherr, M., Callahan, C., Hwang, J. and Ross, C.A. (2000) An autosomal dominant disorder similar to Huntington's disease is associated with a CAG trinucleotide expansion. *Am. J. Hum. Genet.*, **67** (Suppl. 2), 378.
5. Saudou, F., Finkbeiner, S., Devys, D. and Greenberg, M.E. (1998) Huntingtin acts in the nucleus to induce apoptosis but death does not correlate with the formation of intranuclear inclusions. *Cell*, **95**, 55–66.
6. Klement, I.A., Skinner, P.J., Kaytor, M.D., Yi, H., Hersch, S.M., Clark, H.B., Zoghbi, H.Y. and Orr, H.T. (1998) Ataxin-1 nuclear localization and aggregation: role in polyglutamine-induced disease in SCA1 transgenic mice. *Cell*, **95**, 41–53.
7. Cummings, C.J., Reinstein, E., Sun, Y., Antalffy, B., Jiang, Y., Ciechanover, A., Orr, H.T., Beaudet, A.L. and Zoghbi, H.Y. (1999) Mutation of the E6-AP ubiquitin ligase reduces nuclear inclusion frequency while accelerating polyglutamine-induced pathology in SCA1 mice. *Neuron*, **24**, 879–892.
8. Perutz, M.F. (1999) Glutamine repeats and neurodegenerative diseases: molecular aspects. *Trends Biochem. Sci.*, **24**, 58–63.
9. Carmichael, J., Chatellier, J., Woolfson, A., Milstein, C., Fersht, A.R. and Rubinsztein, D.C. (2000) Bacterial and yeast chaperones reduce both aggregate formation and cell death in mammalian cell models of Huntington's disease. *Proc. Natl Acad. Sci. USA*, **97**, 9701–9705.
10. Orr, H.T. and Zoghbi, H.Y. (1998) Polyglutamine tract vs. protein context in SCA1 pathogenesis. In Rubinsztein, D.C and Hayden, M.R. (eds), *Analysis of Triplet Repeat Disorders*. Bios Scientific Publishers, Oxford, pp. 105–117.
11. Young, A., (1999) Huntington's disease and other trinucleotide repeat disorders. In J. Martin (ed.), *Scientific American Molecular Neurology*, Scientific American, Inc., New York.
12. Gossen, M., Freundlieb, S., Bender, G., Muller, G., Hillen, W. and Bujard, H. (1995) Transcriptional activation by tetracyclines in mammalian cells. *Science*, **268**, 1766–1769.
13. Paulson, H.L., Perez, M.K., Trottier, Y., Trojanowski, J.Q., Subramony, S.H., Das, S.S., Vig, P., Mandel, J.L., Fischbeck, K.H. and Pittman, R.N. (1997) Intranuclear inclusions of expanded polyglutamine protein in spinocerebellar ataxia type 3. *Neuron*, **19**, 333–344.
14. Igarashi, S., Koide, R., Shimohata, T., Yamada, M., Hayashi, Y., Takano, H., Date, H., Oyake, M., Sato, T., Sato, A. *et al.* (1998) Suppression of aggregate formation and apoptosis by transglutaminase inhibitors in cells expressing truncated DRPLA protein with an expanded polyglutamine stretch. *Nat. Genet.*, **18**, 111–117.
15. Cooper, J.K., Schilling, G., Peters, M.F., Herring, W.J., Sharp, A.H., Kaminsky, Z., Masone, J., Khan, F.A., Delanoy, M., Borchelt, D.R. *et al.* (1998) Truncated N-terminal fragments of huntingtin with expanded glutamine repeats form nuclear and cytoplasmic aggregates in cell culture. *Hum. Mol. Genet.*, **7**, 783–790.
16. Hackam, A.S., Singaraja, R., Wellington, C.L., Metzler, M., McCutcheon, K., Zhang, T., Kalchman, M. and Hayden, M.R. (1998) The influence of huntingtin protein size on nuclear localization and cellular toxicity. *J. Cell Biol.*, **141**, 1097–1105.
17. Martindale, D., Hackam, A., Wieczorek, A., Ellerby, L., Wellington, C., McCutcheon, K., Singaraja, R., Kazemi-Esfarjani, P., Devon, R., Kim, S.U. *et al.* (1998) Length of huntingtin and its polyglutamine tract influences localization and frequency of intracellular aggregates. *Nat. Genet.*, **18**, 150–154.
18. DiFiglia, M., Sapp, E., Chase, K.O., Davies, S.W., Bates, G.P., Vonsattel, J.P. and Aronin, N. (1997) Aggregation of huntingtin in neuronal intranuclear inclusions and dystrophic neurites in brain. *Science*, **277**, 1990–1993.
19. Davies, S.W., Turmaine, M., Cozens, B.A., DiFiglia, M., Sharp, A.H., Ross, C.A., Scherzinger, E., Wanker, E.E., Mangiarini, L. and Bates, G.P. (1997) Formation of neuronal intranuclear inclusions underlies the neurological dysfunction in mice transgenic for the HD mutation. *Cell*, **90**, 537–548.
20. Wyttenbach, A., Carmichael, J., Swartz, J., Furlong, R.A., Narain, Y., Rankin, J. and Rubinsztein D.C. (2000) Effects of heat shock, heat shock protein 40 (HDJ-2), and proteasome inhibition on protein aggregation in cellular models of Huntington's disease. *Proc. Natl Acad. Sci. USA*, **97**, 2898–2903.
21. Jana, N.R., Tanaka, M., Wang, G.H. and Nukina, N. (2000) Polyglutamine length-dependent interaction of hsp40 and hsp70 family chaperones with truncated N-terminal huntingtin: their role in suppression of aggregation and cellular toxicity. *Hum. Mol. Genet.*, **9**, 2009–2018.
22. Schilling, G., Becher, M.W., Sharp, A.H., Jinnah, H.A., Duan, K., Kotzuk, J.A., Slunt, H.H., Ratovitski, T., Cooper, J.K., Jenkins, N.A. *et al.* (1999) Intranuclear inclusions and neuritic aggregates in transgenic mice expressing a mutant N-terminal fragment of huntingtin. *Hum. Mol. Genet.*, **8**, 397–407.
23. Cummings, C.J., Mancini, M.A., Antalffy, B., DeFranco, D.B., Orr, H.T. and Zoghbi, H.Y. (1998) Chaperone suppression of aggregation and altered subcellular proteasome localization imply protein misfolding in SCA1. *Nat. Genet.*, **19**, 148–154.
24. Chai, Y., Koppenhafer, S.L., Bonini, N.M. and Paulson, H.L. (1999) Analysis of the role of heat shock protein (Hsp) molecular chaperones in polyglutamine disease. *J. Neurosci.*, **19**, 10338–10347.
25. Stenoien, D.L., Cummings, C.J., Adams, H.P., Mancini, M.G., Patel, K., DeMartino, G.N., Marcelli, M., Weigel, N.L. and Mancini, M.A. (1999) Polyglutamine-expanded androgen receptors form aggregates that sequester heat shock proteins, proteasome components and SRC-1, and are suppressed by the HDJ-2 chaperone. *Hum. Mol. Genet.*, **8**, 731–741.
26. Luthi-Carter, R., Strand, A., Peters, N.L., Solano, S.M., Hollingsworth, Z.R., Menon, A.S., Frey, A.S., Spektor, B.S., Penney, E.B., Schilling, G. *et al.* (2000) Decreased expression of striatal signaling genes in a mouse model of Huntington's disease. *Hum. Mol. Genet.*, **9**, 1259–1271.
27. Narain, Y., Wyttenbach, A., Rankin, J., Furlong, R.A. and Rubinsztein, D.C. (1999) A molecular investigation of true dominance in Huntington's disease. *J. Med. Genet.*, **36**, 739–746.
28. Kazantsev, A., Preisinger, E., Dranovsky, A., Goldgaber, D. and Housman, D. (1999) Insoluble detergent-resistant aggregates form

between pathological and nonpathological lengths of polyglutamine in mammalian cells. *Proc. Natl Acad. Sci. USA*, **96**, 11404–11409.
29. Lodi, R., Schapira, A.H., Manners, D., Styles, P., Wood, N.W., Taylor, D.J. and Warner, T.T. (2000) Abnormal *in vivo* skeletal muscle energy metabolism in Huntington's disease and dentatorubropallidoluysian atrophy. *Ann. Neurol.*, **48**, 72–76.
30. Tabrizi, S.J., Workman, J., Hart, P.E., Mangiarini, L., Mahal, A., Bates, G., Cooper, J.M. and Schapira AH (2000) Mitochondrial dysfunction and free radical damage in the Huntington R6/2 transgenic mouse. *Ann. Neurol.*, **47**, 80–86.
31. Hawley, R.J., Scheibe, R.J. and Wagner, J.A. (1992) NGF induces the expression of the VGF gene through a cAMP response element. *J. Neurosci.*, **12**, 2573–2581.
32. Ishida, T., Yamauchi, K., Ishikawa, K. and Yamamoto, T. (1993) Molecular cloning and characterization of the promoter region of the human c-erbA α gene. *Biochem. Biophys. Res. Commun.*, **191**, 831–839
33. Ishidoh, K., Suzuki, K., Katunuma, N. and Kominami, E. (1991) Gene structures of rat cathepsins H and L. *Biomed. Biochim. Acta*, **50**, 541–547.
34. Du, K., Asahara, H., Wagner, B. and Montminy, M. (2000) Characterisation of a CREB gain-of-function mutant with constitutive transcriptional acitivity *in vivo*. *Mol. Cell Biol.*, **20**, 4320–4327.
35. Rich, T., Assier, E., Skepper, J., Segard, H.B., Allen, R.L., Charron, D. and Trowsdale, J. (1999) Disassembly of nuclear inclusions in the dividing cell—a novel insight into neurodegeneration. *Hum. Mol. Genet.*, **8**, 2451–2459.
36. Sherman, M.Y. and Goldberg, A.L. (2001) Cellular defenses against unfolded proteins: a cell biologist thinks about neurodegenerative diseases. *Neuron*, **29**, 15–32.
37. Yoshizawa, T., Yamagishi, Y., Koseki, N., Goto, J., Yoshida, H., Shibasaki, F., Shoji, S. and Kanazawa, I. (2000) Cell cycle arrest enhances the *in vitro* cellular toxicity of the truncated Machado–Joseph disease gene product withan expanded polyglutamine stretch. *Hum. Mol. Genet.*, **9**, 69–78.
38. Ona, V.O., Li, M., Vonsattel, J.P., Andrews, L.J., Khan, S.Q., Chung, W.M., Frey, A.S., Menon, A.S., Li, X.J., Stieg, P.E. *et al.* (1999) Inhibition of caspase-1 slows disease progression in a mouse model of Huntington's disease. *Nature*, **399**, 263–267.
39. Chen, M., Ona, V.O., Li, M., Ferrante, R.J., Fink, K.B., Zhu, S., Bian, J., Guo, L., Farrell, L.A., Hersch, S.M. *et al.* (2000) Minocycline inhibits caspase-1 and caspase-3 expression and delays mortality in a transgenic mouse model of Huntington disease. *Nat. Med.*, **6**, 797–801.
40. Kim, M., Lee, H.S., LaForet, G., McIntyre, C., Martin, E.J., Chang, P., Kim, T.W., Williams, M., Reddy, P.H., Tagle, D. *et al.* (1999) Mutant huntingtin expression in clonal striatal cells: dissociation of inclusion formation and neuronal survival by caspase inhibition. *J. Neurosci.*, **19**, 964–973.
41. Li, S.H., Cheng, A.L., Li, H. and Li, X.J. (1999) Cellular defects and altered gene expression in PC12 cells stably expressing mutant huntingtin. *J. Neurosci.*, **19**, 5159–5172.
42. Francois, F., Godinho, M.J. and Grimes, M.L. (2000) CREB is cleaved by caspases during neural cell apoptosis. *FEBS Lett.*, **486**, 281–284.
43. De Souza, E.B., Whitehouse, P.J., Folstein, S.E., Price, D.L. and Vale, W.W. (1987) Corticotropin-releasing hormone (CRH) is decreased in the basal ganglia in Huntington's disease. *Brain Res.*, **437**, 355–359.
44. Sapp, E., Ge, P., Aizawa, H., Bird, E., Penney, J., Young, A.B., Vonsattel, J.P. and DiFiglia, M. (1995) Evidence for a preferential loss of enkephalin immunoreactivity in the external globus pallidus in low grade Huntington's disease using high resolution image analysis. *Neuroscience*, **64**, 397–404
45. Timmers, H.J., Swaab, D.F., van de Nes, J.A. and Kremer, H.P. (1996) Somatostatin 1–12 immunoreactivity is decreased in the hypothalamic lateral tuberal nucleus of Huntington's disease patients. *Brain Res.*, **728**, 141–148.
46. Augood, S.J., Faull, R.L., Love, D.R. and Emson, P.C. (1996) Reduction in enkephalin and substance P messenger RNA in the striatum of early grade Huntington's disease: a detailed cellular in situ hybridization study. *Neuroscience*, **72**, 1023–1036.
47. Shimohata, T., Nakajima, T., Yamada, M., Uchida, C., Onodera, O., Naruse, S., Kimura, T., Koide, R., Nozaki, K., Sano, Y. *et al.* (2000) Expanded polyglutamine stretches interact with TAFII130, interfering with CREB-dependent transcription. *Nat. Genet.*, **26**, 29–36.
48. Nucifora, F.C.,Jr, Sasaki, M., Peters, M.F., Huang, H., Cooper, J.K., Yamada, M., Takahashi, H., Tsuji, S., Troncoso, J., Dawson, V.L. *et al.* (2001) Interference by huntingtin and atrophin-1 with cbp-mediated transcription leading to cellular toxicity. *Science*, **291**, 2423–2428.
49. McCampbell, A., Taylor, J.P., Taye, A.A., Robitschek, J., Li, M., Walcott, J., Merry, D., Chai, Y., Paulson, H., Sobue, G. and Fischbeck, K.H. (2000) CREB-binding protein sequestration by expanded polyglutamine. *Hum. Mol. Genet.*, **9**, 2197–2202.
50. Giebler, H.A., Lemasson, I. and Nyborg, J.K. (2000) p53 recruitment of CREB binding protein mediated through phosphorylated CREB: a novel pathway of tumor suppressor regulation. *Mol. Cell. Biol.*, **20**, 4894–4858.
51. Saluja, D., Vassallo, M.F. and Tanese, N. (1998) Distinct subdomains of human $TAF_{II}130$ are required for interactions with glutamine-rich transcription activators. *Mol. Cell. Biol.*, **18**, 5734–5743.
52. Barth, A.L., McKenna, M., Glazewski, S., Hill, P., Impey, S., Storm, D. and Fox, K. (2000) Upregulation of cAMP response element-mediated expression during experience-dependent plasticity in adult neocortex. *J. Neurosci.*, **20**, 4206–4216.
53. Usdin, M.T., Shelbourne, P.F., Myers, R.M. and Madison, D.V. (1999) Impaired synaptic plasticity in mice carrying the Huntington's disease mutation. *Hum. Mol. Genet.*, **8**, 839–846.
54. Murphy, K.S.J., Carter, R.J., Lione, L.A., Mangiarini, L., Mahal, A., Bates, G.P., Dunnett, S.B. and Morton, A.J. (2000) Abnormal synpatic plasticity and impaired spatial cognition in mice transgenic for exon 1 of the human Huntington's disease mutation. *J. Neurosci.*, **20**, 5115–5123.
55. Wadzinski, B.E., Wheat, W.H., Jaspers, S., Peruski, J.F.,Jr, Lickteig, R.L, Johnson, G.L. and Klemm, D.J. (1993) Nuclear protein phosphatase 2A dephosphorylates protein kinaseA-phosphorylated CREB and regulates CREB transcriptional stimulation. *Mol. Cell. Biol.*, **13**, 2822–2834.
56. Steffan, J.A., Kazantsev, A., Spasic-Boskovic, O., Greenwald, M., Zhu, Y.-Z., Gohler, H., Wanker, E., Bates, G.P., Housman, D.E. and Thompson, L.M. (2000) The Huntington's disease protein interacts with p53 and CREB-binding protein and represses transcription. *Proc. Natl Acad. Sci. USA*, **97**, 6763–6768.
57. Steward, L.J., Bufton, K.E., Hopkins, P.C., Davies, W.E. and Barnes, N.M. (1993) Reduced levels of 5-HT3 receptor recognition sites in the putamen of patients with Huntington's disease. *Eur. J. Pharmacol.*, **242**, 137–143.
58. Salton, S.R., Ferri, G.L., Hahm, S., Snyder, S.E., Wilson, A.J., Possenti, R. and Levi, A. (2000) VGF: a novel role for this neuronal and neuroendocrine polypeptide in the regulation of energy balance. *Front. Neuroendocrinol.*, **21**, 199–219.
59. Tanaka, K., Pracyk, J.B., Takeda, K., Yu, Z.X., Ferrans, V.J., Deshpande, S.S., Ozaki, M., Hwang, P.M., Lowenstein, C.J., Irani, K. and Finkel, T. (1998) Expression of Id1 results in apoptosis of cardiac myocytes through a redox-dependent mechanism. *J. Biol. Chem.*, **273**, 25922–25928.
60. Tzeng, S.F. and de Vellis, J. (1998) Id1, Id2, and Id3 gene expression in neural cells during development. *Glia*, **24**, 372–381.
61. Rickwood, D., Wilson, M.T. and Darley-Usmar, V.M. (1987) Isolation and characteristics of intact mitochondria. In Darley-Usamr, V.M., Rickwood, D. and Wilson, M.T. (eds), *Mitochondria: A Practical Approach*. IRL Press, Oxford, pp. 1–16.
62. Schapira, A.H.V., Mann, V.M., Cooper, J.M., Dexter, D., Daniel, S.E., Jenner, P., Clark, J.B. and Marsden, C.D. (1990) Anatomic and disease specificity of NADH CoQ1 reductase (complex I) deficiency in Parkinson's disease. *J. Neurochem.*, **55**, 2142–2145.
63. Gardner, P.R., Nguyen, D.D.H. and White, C.W. (1994) Aconitase is a sensitive and critical target of oxygen poisoning in cultured mammalian cells and in rat lungs. *Proc. Natl Acad. Sci. USA*, **91**, 12248–12252.
64. Lowry, O.H., Rosebrough, N.J., Farr, A.L. and Randall, R.J. (1951). Protein measurement with the Folin phenol reagent. *J. Biol. Chem.*, **193**, 265–275.
65. Matoba, R., Kato, K., Saito, S., Kurooka, C., Maruyama, C., Sakakibara, Y. and Matsubara, K. (2000) Gene expression in the mouse cerebellum during its development. *Gene*, **241**, 125–131.
66. Matoba, R., Kato, K., Kurooka, C., Maruyama, C., Sakakibara, Y. and Matsubara, K. (2000b) Correlation between gene functions and developmental expression patterns in the mouse cerebellum. *Eur. J. Neurosci.*, **12**, 1357–1371.
67. Kaminnski, N., Allard, J.D., Pittet, J.F., Zuo, F., Griffiths, M.J. and Morris, D. (2000) Global analysis of gene expression in pulmonary fibrosis reveals distinct programs regulating lung inflammation and fibrosis. *Proc. Natl Acad. Sci. USA*, **97**, 1778–1783.
68. Coles, R., Caswell, R. and Rubinsztein, D.C. (1998) Functional analysis of the Huntington's disease (HD) gene promoter. *Hum. Mol. Genet.*, **7**, 791–800.